Genomics of Preaxostyla Flagellates Illuminates the Path Towards the Loss of Mitochondria

Lukáš V. F. Novák[*1,2], Sebastian C. Treitli[1], Jan Pyrih[1], Paweł Hałakuc[3], Shweta V. Pipaliya[4,5], Vojtěch Vacek[1], Ondřej Brzoň[1], Petr Soukal[1], Laura Eme[6], Joel B. Dacks[4,7], Anna Karnkowska[3], Marek Eliáš[8] & Vladimír Hampl[*1]

[1] Charles University, Faculty of Science, Department of Parasitology, BIOCEV, Vestec, Czech Republic.

[2] Université de Bretagne Occidentale, CNRS, Unité Biologie et Ecologie des Ecosystèmes Marins Profonds BEEP, IUEM, Plouzané, France.

[3] Institute of Evolutionary Biology, Faculty of Biology, Biological and Chemical Research Centre, University of Warsaw, Poland.

[4] Division of Infectious Diseases, Department of Medicine, University of Alberta, Edmonton, Canada.

[5] School of Life Sciences, École Polytechnique Fédérale de Lausanne, Lausanne, Switzerland; Swiss Institute of Bioinformatics, Lausanne, Switzerland.

[6] Ecology, Systematics, and Evolution Unit, Université Paris-Saclay, CNRS, Orsay, France.

[7] Institute of Parasitology, Biology Centre, Czech Academy of Sciences, České Budějovice, Czechia.

[8] University of Ostrava, Faculty of Science, Department of Biology and Ecology, Ostrava, Czech Republic.

* Corresponding author

Abstract

The notion that mitochondria cannot be lost was shattered with the report of an oxymonad *Monocercomonoides exilis*, the first eukaryote arguably without any mitochondrion. Yet, questions remain about whether this extends beyond the single species and how this transition took place. The Oxymonadida is a group of gut endobionts taxonomically housed in the Preaxostyla which also contains free-living flagellates of the genera *Trimastix* and *Paratrimastix*. The latter two taxa harbour conspicuous mitochondrion-related organelles (MROs). Here we report high-quality genome and transcriptome assemblies of two Preaxostyla representatives, the free-living *Paratrimastix pyriformis* and the oxymonad *Blattamonas nauphoetae*. We performed thorough comparisons among all available genomic and transcriptomic data of Preaxostyla to further decipher the evolutionary changes towards amitochondriality, endobiosis, and unstacked Golgi. Our results provide insights into the metabolic and endomembrane evolution, but most strikingly the data confirm the complete loss of mitochondria for all three oxymonad species investigated (*M. exilis*, *B. nauphoetae*, and *Streblomastix strix*), suggesting the amitochondriate status is common to a large part if not whole group of Oxymonadida. This observation moves this unique loss to 100 MYA when oxymonad lineage diversified.

Author summary

Mitochondria are nearly ubiquitous components of eukaryotic cells that constitute bodies of animals, fungi, plants, algae, and a broad diversity of single-celled eukaryotes, *aka* protists. Many groups of protists have substantially reduced the complexity of their mitochondria because they live in oxygen-poor environments, so they are unable to utilize the most salient feature of mitochondria – their ATP-producing oxidative phosphorylation metabolism. However, for a long time, scientists thought that it is impossible to completely lose a mitochondrion because this organelle provides other essential services to the cell, e.g. synthesis of protein cofactors called iron-sulfur clusters. Detailed investigation of chinchilla symbiont M. *exilis* documented the first case of an organism without mitochondrion, and it also provided a scenario explaining how this unique evolutionary experiment might have happened. In this work, we expand on this discovery by exploring genomes of multiple relatives of *M. exilis*. We show that the loss of the mitochondrion is not limited to a single species but possibly extends to its entire group, the oxymonads. We also compare the predicted metabolic capabilities of oxymonads to their closest known mitochondrion-containing relatives and map out various changes that occurred during the transition to amitochondriality.

53 # Introduction

54 Multiple eukaryotic lineages have adapted to low-oxygen and/or endobiotic lifestyles by modifying
55 their mitochondria into a wide range of mitochondrion-related organelle (MRO) types via the
56 process of reductive and adaptive evolution [1]. The most radically modified MROs are
57 traditionally categorized as hydrogenosomes, producing ATP by extended glycolysis, and as
58 mitosomes with no role in energy metabolism [2]. However, exploration of a broader diversity of
59 MRO-containing lineages makes it clear that MROs of various organisms form a functional
60 continuum [3–6]. The extreme outcome of mitochondrial reductive evolution is the complete loss
61 of the organelle, but so far only one organism has been conclusively shown to have reached this
62 point, the chinchilla gut symbiont *Monocercomonoides exilis* (Oxymonadida, Preaxostyla,
63 Metamonada). A genomic project has thoroughly corroborated the amitochondriate status of
64 *M. exilis*, in which it failed to identify any mitochondrion-associated genes while showing multiple
65 other eukaryotic cellular systems to be well represented [7–9].

66 Oxymonadida contains approximately 140 described species of morphologically divergent and
67 diverse flagellates exclusively inhabiting the digestive tracts of metazoans, of which none has been
68 conclusively shown to possess a mitochondrion by cytological investigations [10]. Therefore, the
69 entire Oxymonadida group may be an amitochondriate lineage, with the mitochondrion being lost
70 in its common ancestor. Oxymonads belong to Preaxostyla, one of the five major clades of the
71 phylum Metamonada consisting of exclusively anaerobes or microaerophiles; the other clades are
72 represented by Fornicata (e.g., *Giardia intestinalis*), Parabasalia (e.g., *Trichomonas vaginalis*),
73 barthelonids and their relatives (the BRC group; [11,12]), and Anaeramoebidae (e.g., *Anaeramoeba*
74 *flamelloides*; [13]). The two additional known branches of Preaxostyla, classified as the genera

75 *Trimastix* and *Paratrimastix*, split out at two successive points off the trunk leading to
76 Oxymonadida (Fig 1A). They are both comprised of free-living, bacterivorous flagellates
77 exhibiting a typical excavate morphology and ultrastructure and thriving in low-oxygen
78 environments [14].

79 *Paratrimastix pyriformis* has been shown to possess an MRO morphologically resembling
80 a hydrogenosome. However, it is likely not involved in the ATP-generating extended glycolysis
81 but plays a role in the one-carbon metabolism of the cell [15–17]. Putative MROs have also been
82 observed in electron microscopy studies of a *Trimastix* representative, *T. marina* [14], and their
83 nature was illuminated by transcriptomic data [5]. As a group with at least two MRO-bearing
84 lineages and an amitochondriate species/clade nested within, the Preaxostyla clade provides
85 a promising model system to study the causes, conditions, and consequences of the loss of this
86 ubiquitous cellular compartment.

87 To start answering questions about the timing and circumstances of this single evolutionary
88 experiment in which the mitochondrion was lost from the cell, a denser sampling of omics-level
89 data from Preaxostyla is needed. Currently, the available data encompasses a genome draft of
90 *M. exilis*, transcriptomes of *P. pyriformis* and *T. marina* with variable completeness, and
91 a fragmentary single-cell genome assembly of an oxymonad *Streblomastix strix*. As a key step
92 towards this end, we present high-quality genomic assemblies for another oxymonad, *Blattamonas*
93 *nauphoetae*, and for the free-living *P. pyriformis*. The distribution of mitochondrion hallmark
94 proteins and comparisons of gene repertoires and metabolic functions among five Preaxostyla
95 species of various ecology and MRO status were used to illuminate the adaptations connected to
96 amitochondriality, loss of stacked Golgi, and the origin of endobiotic lifestyle within the group.

97 # Results and discussion

98 **The genome assemblies of *Paratrimastix pyriformis* and *Blattamonas nauphoetae* are highly**
99 **contiguous and nearly complete**

100 We employed a combination of Oxford Nanopore and Illumina technologies to obtain genome
101 assemblies of two species of Preaxostyla. As both species are grown in polyxenic cultures where
102 the eukaryotes represent a minority of cells, we employed multiple rounds of decontamination.
103 Prior to the genomic DNA isolation, enrichment of the sample for the eukaryotic cells was achieved
104 using filtration, and after sequencing the data were carefully decontaminated bioinformatically,
105 resulting in two highly contiguous eukaryotic genome assemblies (see Materials and methods). The
106 basic characteristics of these genomic assemblies and their comparison to the previously published
107 assemblies of Preaxostyla taxa are given in Table 1.

108 The *B. nauphoetae* genome was assembled into 879 contigs spanning 88,537,989 bp, with an
109 N50 = 199,589 bp and a GC content of 44.96%. Automatic and manual gene prediction resulted in
110 25,221 predicted protein-coding genes. The *P. pyriformis* genome was assembled into 633
111 scaffolds spanning 56,627,582 bp, with an N50 = 276,605 bp and a GC content of 60.94%. Manual
112 and automatic gene prediction resulted in 10,815 predicted protein-coding genes.

113 Using BUSCO v3 [18] with the eukaryota_odb9 dataset, the genome completeness was estimated
114 to be 76.3% and 76.6% for *P. pyriformis* and *B. nauphoetae*, respectively (Table 1). BUSCO
115 values, despite their wide usage, are not expected to reach 100% in lineages distant from model
116 eukaryotes simply due to the true absence or high sequence divergence of some of the assessed
117 marker genes. A detailed list of BUSCO markers in Preaxostyla and a comparison of their
118 presence/absence in high-quality genomes of *Trypanosoma brucei*, *Giardia intestinalis*, and

119 *Trichomonas vaginalis* is given in S1 File, Sheet 1. It demonstrates that the absence of many
120 BUSCO markers is generally shared by the three Preaxostyla species indicating that this is true
121 absence of the given gene in the genome rather than reflection of data incompleteness. To avoid
122 a bias caused by evolutionary divergence, we also attempted to estimate genome completeness
123 using reference-independent approaches with Merqury [19]. Using this method, we obtained
124 a completeness of 94.01% and 98.24% for *P. pyriformis* and *B. nauphoetae*, respectively (Table 1).
125 Finally, we also searched for 79 conserved ribosomal proteins [20]. We identified 74 of them in
126 the predicted gene set of *P. pyriformis*, with the remaining five identified by manual searches in
127 the genome (S1 File, Sheet 2). A comparable result was achieved for *B. nauphoetae*, where we
128 identified 76 of the ribosomal proteins in the predicted gene set, and the remaining three were
129 identified by a manual search in the genome (S1 File, Sheet 3). Altogether our analyses suggest
130 that the *P. pyriformis* and *B. nauphoetae* genome drafts are highly complete.

131 **A systematic search for proteins associated with the mitochondrion fails to identify**
132 **convincing candidates in oxymonads**

133 The hypothesis of the mitochondrion organelle absence in *M. exilis* was postulated based on the
134 absence of mitochondrion-related proteins in its genome and transcriptome and led to overturning
135 of the paradigm that mitochondria are ubiquitous among eukaryotes [7]. Obviously, the
136 amitochondriate status of *M. exilis* is immediately falsifiable by finding any evidence of a putative
137 organelle in this species. Careful inspection of the predicted proteomes of other oxymonads for the
138 presence of mitochondrial hallmarks is an obvious next step that may further support, or weaken,
139 this hypothesis. To follow this line of investigation, we have carefully searched the genome drafts
140 of *P. pyriformis* and *B. nauphoetae* published in this study, the previously published genome drafts
141 of *Monocercomonoides exilis* [7,21] and *Streblomastix strix*, and the previously published

142 transcriptome of *Trimastix marina* [5], i.e., a composite dataset containing three oxymonad species
143 and two other free-living Preaxostyla, the latter clearly possessing an MRO [5,17].

144 We used several methods to identify candidate mitochondrial proteins (results for all searches are
145 shown in S2 File and summarized in Fig 1B and C). In most cases, proteins identified in the first
146 step were searched against the custom mitochondrial protein sequence database based on the
147 MitoMiner database [22,23] (herein referred to as MitoMiner) and those with hits were considered
148 as candidate mitochondrial proteins. In the last step the functional annotation of the candidates
149 based on NCBI best hits or additional hint, co-occurrence across Preaxostyla, were considered to
150 select the putative mitochondrial proteins from the candidates. For the purpose of the analyses the
151 predicted proteins of Preaxostyla were clustered with predicted proteins of other Metamonada into
152 orthologous group (S3 File).

153 **The absence of mitochondrial hallmark genes in oxymonads extends beyond *M. exilis***

154 As the most obvious approach, we searched all five investigated species for homologues of nuclear
155 genome-encoded proteins typically associated with mitochondria or MROs in other eukaryotes
156 including *Paratrimastix* and *Trimastix*. In the first step, we used profile Hidden Markov Models
157 (HMMs) to search for components of the mitochondrion protein import and maturation machinery,
158 considered one of the most conserved mitochondrial features [24]. Homology searches resulted in
159 22 (*T. marina*) to 63 (*M. exilis*) hits, which were further evaluated by searches against the
160 MitoMiner resulting in 57 candidates in total. Functional annotations indicated that all candidates
161 recovered in oxymonad data sets are very likely false positives: mainly vaguely annotated kinases,
162 peptidases, and chaperones (Fig 1B, S2 File). For *P. pyriformis* and *T. marina*, the situation was
163 different. Out of the 11 previously identified components of the *P. pyriformis* mitochondrion
164 protein import and maturation machinery [16,17], 10 were found in the predicted proteomes of

165 these two species with this approach: the β-barrel outer membrane translocases Tom40 and Sam50
166 and the associated receptor Tom22, the inner membrane translocases Tim17, Tim22 and their
167 associated protein Pam18 and Tim44, the α and β subunit of the mitochondrial processing peptidase
168 (MPP), and the mitochondrial chaperone protein HSP70. Tim17 and mtHsp70 were also identified
169 in the *T. marina* dataset, corroborating previous findings [5]. The only exception was the
170 previously detected Tim23 protein (PAPYR_1418; [17]), which was missed in our new search
171 because of high divergence. The successful identification of the protein translocon components in
172 these two species validated our approach.

173 The sensitive HMM searches were complemented by an extensive search for putative homologues
174 of known mitochondrial proteins using a pipeline based on the MitoMiner database (S2 File). As
175 already shown for *M. exilis*, the specificity of the pipeline in organisms with divergent
176 mitochondria is low [7]. The search recovered a similar number of hits in all investigated species,
177 from 636 in *S. strix* up to 1,024 in *P. pyriformis*. An objective assessment of the localization of all
178 these proteins is not realistic. Many of them are clearly not mitochondrial (e.g., histones or
179 ribosomal proteins), and others belong to very general gene ontology categories (e.g., protein-
180 binding) making the assessment impossible. After individually inspecting the remaining items, we
181 conclude there is none among the hits from oxymonads that would raise a strong case for the
182 presence of mitochondria. On the other hand, reliable mitochondrial proteins were found among
183 hits from *P. pyriformis* and *T. marina*. The first such examples are dynamin-like proteins
184 (PAPYR_3413 and Gene.668::gnl|Trimastix_PCT|268). Their phylogenetic position (S4A File)
185 corroborates the hypothesis of Karnkowska et al. [8] that these may mediate the division of MROs
186 in these species. Other examples are proteins (PAPYR_2826 and
187 Gene.3674::gnl|Trimastix_PCT|1191) orthologous to the mitochondrial outer membrane-anchored

188 protein MIRO (mitochondrial Rho; [25]) broadly conserved in eukaryotes but rare in
189 MRO-containing taxa [26,27]. Indeed, PAPYR_2826 was recently confirmed by proteomics to be
190 MRO-associated in *P. pyriformis* [17]. Finally, the search recovered homologues of mitochondrial
191 matrix chaperones Cpn60 and Cpn10 and homologues of mitochondrial carrier family proteins
192 used for export or import ATP and other metabolites [28]. Bacterial-type (NTT-like) nucleotide
193 transporters [29], sporadically used for ATP transport, were not recovered neither by this search
194 nor by targeted BLAST searches.

195 **Homology-independent searches do not identify convincing candidates for mitochondrial**
196 **proteins in the sequenced oxymonad genomes**

197 As an alternative to homology searches, we also searched our Preaxostyla sequence datasets for
198 several types of signature sequences typical for mitochondrion-targeted proteins. The matrix
199 proteins of mitochondria and MROs are expected to contain characteristic N-terminal targeting
200 signals (NTS) needed for the targeted import into MROs [30]. However, it has been previously
201 recognized that the presence of a predicted NTS by itself does not prove the targeting, as such
202 amino acid sequences can also appear by chance [31]. Indeed, we have previously shown that 14
203 *M. exilis* proteins are imported into hydrogenosomes when heterologously expressed in *T. vaginalis*
204 [32]. Here we used TargetP v1.1 and MitoFates v1.1 for mitochondrial targeting signal prediction
205 and identified from as little as two hits in *S. strix* up to 248 hits in *B. nauphoteae* (S2 File). Only
206 21 of these oxymonad sequences found hits in MitoMiner rendering them candidates which were
207 considered further and annotated by BLAST searches against the NCBI nr database (Fig 1B). None
208 of these annotations strongly suggest a mitochondrial function. As an additional hint, we
209 considered the conservation of NTS prediction across Preaxostyla. We reasoned that if the NTS in
210 the protein is real it should be detected also in orthologues from other Preaxostyla species. Only

211 four proteins from oxymonads (ribosomal protein L21, L23a, L34e, and tRNA-dihydrouridine
212 synthase) fulfilled this criterion, none of them representing a reasonable mitochondrial protein in
213 organisms that certainly lack a mitochondrial genome. Based on these results, we assume that all
214 NTS predictions on oxymonad proteins are false positives. Altogether, 50 of *P. pyriformis* and
215 *T. marina* proteins with predicted NTS found hits in MitoMiner rendering them candidates. This
216 probably reflects the presence of the organelle. Indeed, we identified among them, for example,
217 aminoadipate-semialdehyde dehydrogenase, GCS-H, and mtHSP70 proteins all previously
218 suggested to localize to the MRO [5].

219 The outer mitochondrial membrane accommodates two special classes of proteins, TA proteins and
220 mitochondrial β-barrel membrane proteins (MBOMPs), the former using specific C-terminal
221 signals [33–35]. We identified up to 475 TA hits in the predicted proteome of *S. strix* and around
222 100 for the rest of the species, with only 25 for *T. marina* (S2 File). Depending on the species only
223 five to 12 were considered as mitochondrial candidates (i.e. having hits in the MitoMiner database)
224 (Fig 1B) and the majority of these were Golgi apparatus/ER-related upon closer scrutiny. Like in
225 the case of NTS-containing proteins, we assessed if the set of predicted TA proteins contains groups
226 of orthologues containing more than a single Preaxostyla species. Indeed, 22 such orthologous
227 groups were found. These were mostly without MitoMiner hits and in most cases annotated as
228 SNARE or other proteins involved in vesicle trafficking outside mitochondria. This suggests that
229 the TA prediction did produce true positives but they most likely represent non-mitochondrial TA
230 proteins. The only robust mitochondrial candidate from the whole list was Fis1 (mitochondrial
231 fission protein 1) in *T. marina*, which is a tail-anchored (TA) protein mediating mitochondrial
232 fission [36].

233 Our search for proteins with MBOMP characteristics revealed six and 23 hits in *T. marina* and
234 *P. pyriformis*, respectively, but only three of them had a hit in the MitoMiner database, including
235 the *P. pyriformis* Tom40, the detection of which validated our approach (Fig 1B). Among the hits
236 from the oxymonad genomes, only four hit a protein in the MitoMiner database rendering them
237 mitochondrial candidates, none of them being a known MBOMP (S2 File). Only 10 orthologous
238 groups predicted as MBOMPs contained representatives of more than one Preaxostyla species. The
239 annotations of none of them suggested a mitochondrial function: clathrin heavy chain, kelch-type
240 beta-propeller, EF-hand domain-containing protein, eukaryotic translation initiation factor
241 3 subunit B, and BTB/POZ domain-containing protein. The only positive case from this set thus
242 remained Tom40 in *P. pyriformis*.

243 **Probing the oxymonad genomes with the *T. brucei* reference mitochondrial proteome**
244 **provides further support for the absence of mitochondria in oxymonads**

245 Given the limitations of the previous searches, namely, high false-positive rates, uncertainty about
246 mitochondrial localization of proteins included in the MitoMiner database, and the inability to
247 distinguish between the cytosolic and mitochondrial isoforms, we have performed yet another
248 analysis in which we used a carefully curated set of queries. In this analysis, we searched for
249 Preaxostyla orthologues of proteins from the experimentally well-established mitochondrial
250 proteome of *Trypanosoma brucei* [37–40]. The selection of this organism as a reference also
251 considered the fact that it is a member of the eukaryotic supergroup Discoba, which frequently
252 forms a sister group to Metamonada in phylogenomic analyses [41], making *T. brucei* potentially
253 the closest relative of metamonads out of all eukaryotes with extensively studied mitochondria.
254 Reciprocal BLAST searches of the *T. brucei* mitochondrial proteins against the predicted proteins
255 of Preaxostyla revealed ~200 putative groups of orthologues and those were investigated manually.

256 Careful inspection of the raw localization data in *T. brucei* and protein phylogenies rejected most
257 cases by disputing either the mitochondrial localization in *T. brucei* or the orthology; the latter was
258 considered uncertain if *T. brucei* and Preaxostyla proteins were separated by prokaryotic or non-
259 mitochondrial eukaryotic homologues in the phylogenetic trees (S5 File). The 30 cases passing this
260 initial scrutiny (S2 File) were divided into two groups.

261 The high-confidence group comprises 17 proteins that likely share mitochondrial origin as they
262 formed a monophyletic cluster with other mitochondrial homologues. These were present only in
263 *P. pyriformis* and/or *T. marina* and never in oxymonads. Out of these 17 proteins, 12 were already
264 predicted to be mitochondrial previously [17]. The remaining proteins, such as L-threonine
265 3-dehydrogenase (TDH) or glycine acetyltransferase, are thus promising novel candidates for
266 mitochondrial proteins in these two protists.

267 The 13 putative mitochondrial proteins in the low confidence group clustered with known
268 mitochondrial proteins or proteins predicted to reside within the mitochondrion using the TargetP
269 v1.1 algorithm, although the support for the mitochondrial targeting of proteins within these
270 clusters was not consistent. All of such clusters also included cytosolic or peroxisomal isoforms or
271 the enzymes known to be dually localized, which questions the mitochondrial origin of these
272 clusters. An example of the former is isocitrate dehydrogenase, for which the yeast cytosolic,
273 peroxisomal, and mitochondrial proteins form a clade in the tree (S5 File). Examples of the latter
274 are aconitase and alanine aminotransferase, for which a dual cytosolic/mitochondrial location was
275 reported for various eukaryotes including trypanosomatids [42,43]. This low confidence group
276 contained nine proteins present also in oxymonads (S2 File), and these are discussed in more detail
277 below.

278 Aspartate and alanine aminotransferases and the two tRNA synthetases in this category are all
279 dually localized in the mitochondrion and the cytosol of *T. brucei*. In the case of the tRNA
280 synthetases, the dual localization arose specifically in trypanosomatids [39] and, consistently with
281 this hypothesis, Preaxostyla and *T. brucei* proteins cluster together with cytosolic tRNA
282 synthetases of other eukaryotes. In the case of aspartate aminotransferase, the dual localization
283 seems to be of a deeper evolutionary origin [44]. The two mevalonate pathway enzymes
284 (hydroxymethylglutaryl-CoA synthase and 3-hydroxy-3-methylglutaryl-CoA reductase) are
285 localized in the mitochondrion of kinetoplastids [45], however, this is a specialty of this lineage,
286 as eukaryotes typically run this pathway in the cytosol/ER. In all these cases, we conservatively
287 assume that these enzymes were localized in the cytosol in the common ancestor of Preaxostyla
288 and *T. brucei* and were partially or fully moved to the mitochondrion in the lineage leading to
289 *T. brucei*. The last candidate was the malic enzyme. There are two homologues of the enzyme in
290 kinetoplastids, one cytoplasmic and one mitochondrial, which cluster together (S4B File). Again,
291 it cannot be inferred what the situation in the common ancestor with Preaxostyla was, which does
292 not give a strong reason to assume MRO localization in Preaxostyla.

293 In summary, our systematic searches for MRO proteins allowed us to update the predicted set of
294 MRO-localized proteins of *P. pyriformis* and *T. marina* and to provide updated predictions of their
295 MRO proteomes (S6 File). Most critically, no reliable candidate for an MRO protein was detected
296 in any of the oxymonad data sets, supporting the hypothesis of the absence of the mitochondrion
297 in *M. exilis* and, importantly, extending the amitochondriate status to two other oxymonad species.
298 After this new revelation, we wondered how the loss of mitochondria in the three oxymonads
299 species had seeped into functions related to this organelle, namely: extended glycolysis, amino acid
300 metabolism, inventory of FeS cluster-containing proteins, heme synthesis, and peroxisomes.

301 **Inventory of enzymes for extended glycolysis shows a richer diversity of FeFe hydrogenases**
302 **in *Trimastix* and *Paratrimastix* than in oxymonads**

303 Many eukaryotic anaerobes, including Preaxostyla, generate ATP using the extended glycolysis
304 pathway, which produces acetate, CO_2, and H_2 from pyruvate while performing substrate-level
305 phosphorylation of ADP to ATP [46]. The pathway uses pyruvate as a substrate, which is either
306 directly sourced from glycolysis or produced by decarboxylation of malate through the activity of
307 the malic enzyme (ME), which was identified in all five Preaxostyla species. All studied
308 Preaxostyla species apparently rely on oxidative decarboxylation of pyruvate to acetyl coenzyme
309 A (acetyl-CoA) and CO_2 in a reaction catalyzed by pyruvate:ferredoxin oxidoreductase (PFO;
310 [47]), owing to the identification of three to six PFO isoforms in each species analyzed (Fig 2, S4C
311 File, S6 File). None of the alternative enzymes mediating the conversion of pyruvate to acetyl-
312 CoA, pyruvate:NADP+ oxidoreductase (PNO) and pyruvate formate lyase (PFL), could be
313 detected in any of the studied species.

314 Both the decarboxylation of malate by ME and of pyruvate by PFO are oxidative processes that
315 release electrons, producing NADH and reduced ferredoxin, respectively, and these electron
316 carriers need to be reoxidized. The final fate of the electrons carried by ferredoxin often lies in the
317 reduction of protons to molecular hydrogen through the activity of [FeFe] hydrogenases (HydA;
318 [48]). In addition to the "simple" hydrogenases, which are present in all species of Preaxostyla,
319 [FeFe] hydrogenases with N-terminal homology to the NuoG subunit of NADH-quinone
320 oxidoreductase and a C-terminal homology to NADPH-dependent sulfite reductase (CysJ), were
321 identified in the MRO-containing *T. marina* and *P. pyriformis* (Fig 3, S4D File). Similar "fused"
322 hydrogenases have been previously reported in other eukaryotic anaerobes, including *T. vaginalis*
323 [49], the breviate *Pygsuia biforma* [50], the jakobid *Stygiella incarcerata* [51], and the amoebozoan

324 *Pelomyxa schiedti* [52]. Although they do not belong to the group of A3 trimeric hydrogenases
325 [53] known to be capable of NADH oxidation via electron confurcation [54], they were
326 hypothesized to catalyze NAD(P)H-dependent formation of H_2 [49]. Although the presence of
327 these large hydrogenases correlates with the presence of MROs, they were not detected in the MRO
328 proteome of *P. pyriformis* [17] and their localization is unknown.

329 The second reaction of the extended glycolysis, which yields ATP, acetate, and CoA, can be
330 catalyzed either by a two-enzyme system consisting of acetate:succinate CoA-transferase (ASCT)
331 and succinyl CoA synthetase (SCS) like in *T. vaginalis*, or by a single enzyme acetyl-CoA
332 synthetase (ACS) like in *G. intestinalis*. All five Preaxostyla species contain ACS, while neither
333 ASCT nor SCS was identified. ACS has a complicated evolutionary history in Metamonada
334 characterized by multiple LGT events and gene losses [5,11,55]. The majority of ACS homologues
335 in Metamonada are predicted to function in the cytosol, with the only exception of the ACS2
336 isoform from *S. salmonicida* that functions in the MRO [5,56]. Phylogenetic analysis of
337 Preaxostyla ACSs (S4E File) shows four unrelated clades, none in close relationship to the
338 *S. salmonicida* MRO homolog, hinting at a cytosolic localization of these enzymes in Preaxostyla.

339 **Amino acid metabolism is richer in *Trimastix* and *Paratrimastix* than in oxymonads**

340 We noticed clear differences between oxymonads on one side and MRO-containing species
341 *T. marina* and *P. pyriformis* on the other with respect to their amino acid metabolism. Hypothetical
342 amino acid metabolism was reconstructed based on the metabolic maps in the KEGG database and
343 catalytic activities of enzymes reported from other metamonads (S1-3 Fig; [57,58]). The capacity
344 to *de novo* synthesize protein-building amino acids seems larger in *P. pyriformis* (cysteine, serine,
345 glycine, threonine, and selenocysteine) than in oxymonads (cysteine, serine, and selenocysteine
346 only). The inferred capacity of *T. marina* to synthesize only two amino acids (cysteine and

347 selenocysteine) most likely reflects the incompleteness of the sequence data available. The
348 selenocysteine biosynthesis pathway present in *P. pyriformis*, *T. marina*, and *M. exilis* is notable,
349 as the capacity to synthesize this amino acid has been reported only in *S. salmonicida* among other
350 metamonads studied so far [58].

351 Like many other metamonads [59], *M. exilis* has been suggested to utilize arginine for ATP
352 production via the arginine deiminase pathway consisting of three enzymes: arginine deiminase
353 (ADI), carbamate kinase (CK), and ornithine transcarbamylase (OTC). This important metabolic
354 capability has been probably formed in the common ancestor of Metamonada by the acquisition of
355 genes for ADI and OTC via LGT [59]. Here we show the presence of the complete arginine
356 deiminase pathway also in *T. marina* and *B. nauphoetae*, while *P. pyriformis* and *S. strix* lack ADI
357 and CK, respectively. This suggests that ATP production via arginine catabolism is widespread but
358 not omnipresent in Preaxostyla, and it is present in both free-living and endobiotic representatives.
359 Other amino acids can be used in energy metabolism as well: cysteine, serine, and tryptophan can
360 be converted to pyruvate, while methionine can be converted to α-keto-butyrate. Both products
361 then can be used by PFO and ACS to generate ATP [60].

362 Of note is the part of amino acid metabolism connected to the folate and methionine cycle.
363 Methionine (in the form of S-adenosylmethionine, SAM), consumed in reactions catalyzed by
364 SAM-dependent methyltransferases, can be regenerated in the methionine cycle, which is present
365 in *P. pyriformis* and *T. marina* but not identified in any of the three oxymonads. The presence of
366 the methionine cycle is probably connected with the presence of MROs containing a complete
367 glycine cleavage system (GCS) and serine hydroxymethyl transferase (SHMT) in *P. pyriformis*
368 [17] and hypothetically also in *T. marina*. The methyl residues liberated from glycine and serine
369 inside MRO enter the folate cycle and can be later utilized for the methylation of homocysteine to

370 produce methionine via MetH [61]. Oxymonads lack the folate and methionine cycles as well as
371 GCS and SHMT, which is in line with the fact that the latter enzymes are restricted to the
372 mitochondrial compartment in eukaryotes. The transsulfuration pathway, associated with the folate
373 and methionine cycles in mammals [62], was not found in any Preaxostyla species.

374 Our search for components of the GCS in Preaxostyla led us to identifying a protein that constitutes
375 a potential adaptation to the anaerobic lifestyle more broadly shared by multiple unrelated
376 anaerobic eukaryote lineages. Phylogenetic analysis of homologues of the L protein (GCS-L)
377 divided the sequences from Preaxostyla into two clusters (S4F File). The previously characterized
378 MRO-localized protein of *P. pyriformis* considered to function as a bona fide GCS subunit
379 (PAPYR_5544; [17]) branched with sequences of *T. marina*, Parabasalia, and the fornicate
380 *Carpediemonas membranifera*, suggesting that these proteins may be localized in MRO of these
381 species since their common ancestor. Another *P. pyriformis* gene (PAPYR_1328) and its
382 homologues from the oxymonads *M. exilis* and *B. nauphoetae* branched with high statistical
383 support together with sequences from Archamoebae (*Mastigamoeba balamuthi* and *P. schiedti*)
384 and another eukaryotic anaerobe, *Breviata anathema* (Breviatea); we refer to this divergent clade
385 as GCS-L2. Localization of this protein in *P. pyriformis* could not be established as it was measured
386 only in one replicate of the proteomic experiment [17], but given the lack of an N-terminal
387 extension that could potentially serve as a targeting signal into the MRO, we hypothesize it is
388 localized outside this organelle. The well-supported relationship between the GCS-L2 sequences
389 from Preaxostyla, Archamoeabae, and Breviatea may be explained by a eukaryote-to-eukaryote
390 LGT, although the direction of the transfer among the three eukaryote lineages is unknown.
391 Notably, the *M. balamuthi* GCS-L2 protein was encountered before and suggested to function
392 outside the context of the GCS [63], a notion corroborated here by the identification of its close

393 relatives in oxymonads that lack homologues of the other GCS components. It should be noted
394 that, besides GCS, GCS-L (proper) is known to be part of three other protein complexes, pyruvate
395 dehydrogenase, branched-chain amino acid dehydrogenase, and 2-oxoglutarate dehydrogenase
396 [64], none of them being present in Preaxostyla. Outside of these typical roles or under specific
397 conditions, GCS-L was shown to have a moonlighting proteolytic activity [65] or a diaphorase
398 activity by which it oxidizes NADH using labile ferric iron [66], nitric oxide [67], or ubiquinone
399 [68]. It is, therefore, possible that one of these moonlighting activities may represent the primary
400 role of GCS-L2.

401 **Oxymonads use almost exclusively 4Fe-4S clusters in their iron-sulfur clusters containing**
402 **proteins**

403 Fe-S clusters are ancient and versatile inorganic cofactors used by virtually all living organisms
404 and in eukaryotes mostly present in the rhombic 2Fe-2S or cubane 4Fe-4S forms [69]. In a typical
405 eukaryotic cell, Fe-S clusters are synthesized by a combination of the mitochondrial ISC and the
406 cytosolic CIA pathway, but members of Preaxostyla combine the CIA pathway with the SUF
407 pathway acquired by LGT from bacteria to perform the same task [69,70]. The enzymes were
408 shown to localize in the cytosol [17] and the first functional details of the Fe-S cluster biogenesis
409 in this group were described recently [71]. This major pathway shift in the Preaxostyla common
410 ancestor was likely a preadaptation for the loss of the mitochondrion in the lineage leading to
411 *M. exilis* [7].

412 To assess how much the change in the Fe-S cluster assembly pathway affected the inventory of
413 Fe-S cluster-containing proteins in Preaxostyla, we compared the previously predicted Fe-S
414 proteins of *M. exilis* [8] with a set of Fe-S proteins newly predicted from *in silico* proteomes of
415 *P. pyriformis*, *T. marina*, *B. nauphoetae*, and *S. strix* (S7 File). The numbers of Fe-S cluster-

416 containing proteins identified in individual species varied from 48 in *T. marina* (most likely an
417 underestimate of the real number, owing to the incompleteness of the data) to 93 in *P. pyriformis*
418 and are thus not decreased in comparison to other heterotrophic eukaryotes [72]. The predicted
419 Fe-S proteins fell into 164 distinct orthologous groups. The numbers of these OGs shared by
420 different combinations of Preaxostyla species are shown in S4 Fig. The most widespread types of
421 Fe-S cluster-containing proteins in Preaxostyla fall into expected functional groups acting in
422 processes of extended glycolysis and electron transfer (PFO, HydA, ferredoxins, and flavodoxin-
423 ferredoxin domains containing proteins), DNA replication and repair, transcription and translation
424 (e.g., DNA and RNA polymerases, Rli1p), Fe-S cluster assembly itself (SufDSU, SufB, Nbp35,
425 and NAR-1), and nucleotide (XDH) and amino acid metabolism (L-serine dehydratase).

426 Most of the predicted Fe-S proteins in oxymonads contain 4Fe-4S clusters, with the single
427 exception of xanthine dehydrogenase (XDH), which contains both 2Fe-2S and 4Fe-4S clusters.
428 The free-living *P. pyriformis* and *T. marina* furthermore contain other proteins with 2Fe-2S
429 clusters, such as [FeFe] hydrogenases and 2Fe-2S ferredoxin. As the 2Fe-2S cluster occur more
430 frequently in mitochondrial proteins, the higher number of 2Fe-2S proteins in *P. pyriformis*
431 compared to the oxymonads may reflect the presence of the MRO in this species and its absence
432 in oxymonads.

433 **Peroxisomes and pathways for the synthesis of heme are absent in all Preaxostyla**

434 Besides modifications or a complete loss of mitochondria, living in low-oxygen environments
435 and/or living inside hosts typically impacts also peroxisomes. While in most
436 anaerobic/microaerophilic species, including all previously investigated Metamonada, the
437 peroxisomes are absent, both free-living and parasitic Archamoebae recently turned out to possess
438 modified versions of this organelle [73–75], as does *Proteromonas lacertae*, a stramenopile that

439 possesses the most reduced but seemingly functional peroxisomal organelle yet reported [76].
440 Specific genetic markers for the presence of peroxisomes are peroxins, a set of proteins involved
441 in peroxisome biogenesis [77]. Peroxins are absent in the genome of the oxymonad *M. exilis* with
442 a single exception of a divergent homologue of Pex19 [8]. This protein acts as a soluble cytoplasmic
443 receptor for peroxisomal tail-anchored (TA) membrane proteins, which are inserted into the
444 peroxisomal membrane with the help of the Pex3 anchor. The absence of a discernible Pex3
445 homologue in *M. exilis* indicates that the Pex19 homologue is involved in another cellular process.
446 To map the situation in other Preaxostyla, we searched all datasets for homologues of human
447 peroxins (S8 File). Besides putative homologues of Pex19, which were recovered in all species
448 besides *S. strix*, and a Pex3 homologue recovered in *P. pyriformis*, no other peroxins were detected.
449 The Pex3/Pex19 pair in *P. pyriformis* was already reported by Zítek et al. [17], who provided
450 proteomic evidence for Pex3 being localized in the MRO and hypothesized that the Pex3/Pex19
451 system is involved in the targeting of TA proteins into the outer MRO membrane. Altogether, the
452 results of our searches do not indicate the presence of peroxisomes in Preaxostyla lineage. Thus,
453 the apparent absence of Pex3 in oxymonads seems to be another trait linked to the loss of the
454 mitochondrion in these organisms.

455 The modification of mitochondria for life in low-oxygen environments typically leads to the loss
456 of the capacity for the synthesis of heme [78], a cofactor of many proteins involved in redox
457 reactions, namely the complexes of the respiratory chain. Preaxostyla are no exception in this
458 respect as no homologues of these enzymes were identified in their datasets. Still, cytochrome b5
459 domain-containing proteins were recovered in all Preaxostyla (S6 File) indicating that they use
460 hemoproteins and likely sequester heme from the food.

461 **Membrane transporter complement may reflect adaptation to an endobiotic lifestyle in**
462 **oxymonads**

463 The collected -omic data set from Preaxostyla allows us to examine two other evolutionary changes
464 besides the loss of the mitochondrion, the transition from a free-living to an endobiotic lifestyle
465 and the loss of stacked Golgi. Although all three events occurred on the same branch of the
466 phylogenetic tree, leading to the common ancestor of the three analyzed oxymonads, we have no
467 clear evidence that they are directly related. However, an indirect link between them is possible.
468 For example, the transition to an endobiotic mode of life could cause the loss of the methionine
469 cycle in oxymonads. This change might subsequently allow for the loss of mitochondria, whose
470 only essential role in free-living Preaxostyla species is to provide methyl groups for this cytosolic
471 cycle [17].

472 To assess genetic trace of the transition to endobiotic lifestyle, we examined proteins responsible
473 for the transport of metabolites and other chemicals across the plasma membrane and other cell
474 membranes. We searched for a broad spectrum of transmembrane transporters (except for
475 transporters of MROs) using homology-based methods in order to compare the repertoire of
476 functional types as well as the number of paralogues between the five species of Preaxostyla (S9
477 File).

478 The most gene-rich group of membrane transporters identified in Preaxostyla is the ATP-binding
479 cassette (ABC) superfamily represented by MRP and pATPase families, just like in *T. vaginalis*
480 [57]. Altogether, representatives of 19 transporter families have been identified in Preaxostyla. All
481 of them are present in both free-living species *P. pyriformis* and *T. marina*, while four families
482 (PotE, SPNS, RFC, and TauE) are missing in all three endobiotic oxymonads investigated. On the
483 other hand, transporters of nucleosides, sugars, amino acids, choline, and phospholipids have

484 consistently higher numbers of paralogues in the genomes of the oxymonads *M. exilis* and
485 *B. nauphoetae* than in *P. pyriformis* and their phylogenetic trees are consistent with gene family
486 expansion in oxymonads (S4G–K File). These two observations parallel the findings of functional
487 domain loss and expansion by gene duplication of transporter families in Microsporidia [79],
488 possibly hinting at a broader evolutionary pattern at the transition to the endobiotic lifestyle.
489 Indeed, gene duplication in specific types of transmembrane transporters may be a common
490 adaptation at the transition to a new environment in eukaryotes; for example, expansion in gene
491 families encoding ion transporters has been observed in halophilic organisms [80–82] when
492 compared to their mesophilic relatives.

493 **Evidence from the Golgi complex-associated protein complement in Preaxostyla is consistent**
494 **with the cisternal adhesion model of Golgi stacking**

495 Another evolutionary transition addressable by our results is the presence of a morphologically
496 identifiable Golgi body in *P. pyriformis* and *T. marina* versus the lack in oxymonads [14,21,83].
497 This absence of a morphologically identifiable Golgi-homologue and yet the detection of
498 a substantial complement of proteins associated with Golgi membrane-trafficking and transport
499 was used in the initial Karnkowska et al. 2016 paper to provide evidence for a Golgi body, in the
500 oxymonad *M. exilis* [7,8], serving as a positive control for the informatic ability to detect genomic
501 signals of cryptic organelles. Golgi bodies with non-canonical morphologies are relatively rare in
502 eukaryotes, as compared with the hallmark stacked cisternal form [84]. However, such organelles
503 are well-documented [84]. Surprisingly, the molecular basis for the canonical eukaryotic stacked
504 morphology is unclear. Many proteins have been implicated in Golgi stacking, though none yet
505 found to be universal. At the same time the cisternal adhesion model [85], an emerging but still
506 relatively controversial theory, proposes that a sufficient amount of any one of several putative

507 stacking factors could provide the adhesive property to keep the stacks together. A 2018 study by
508 Barlow et. al. [86], looked for all proposed Golgi-stacking factors at the time by sampling genomic
509 data from across eukaryotes possessing stacked and unstacked Golgi morphologies. No protein was
510 found in a pattern that supported it as a necessary and sufficient for Golgi stacking, although the
511 complement of Golgins inferred to be present in LECA did support the functional distinction of cis
512 vs trans-Golgi. This finding was most consistent with the cisternal adhesion model. Nonetheless,
513 the organisms sampled with divergent Golgi morphologies were still quite distantly related and
514 thus the evidence supporting the model was still relatively weak.

515 By contrast, our dataset represents one of the tightest samplings to date where genomic data is
516 available for the closest known species on both sides of the divide between stacked and unstacked
517 Golgi morphology. Consequently, we searched in our datasets to assess the Golgi complement in
518 the additional Preaxostyla representatives, particularly to see whether the complement was more
519 extensive in the organisms possessing stacked Golgi bodies.

520 The scope of our examination included proteins involved in vesicle formation, vesicle fusion, and
521 the golgin proteins implicated in Golgi structure [87–92]. We observed near complete complements
522 of the COPI, AP1, AP3, AP4, and Retromer vesicle coats, as well as the GARP complex, Trs120,
523 and syntaxins 5 and 16 (Fig 4, S6 File). We also noted at least one golgin protein in each of the
524 organisms. Indeed, we observed additional paralogues of the vesicle trafficking machinery (e.g.,
525 AP1, Retromer, GARP/EARP) in oxymonads compared to *P. pyriformis* and *T. marina*, (Fig 4, S6
526 File). These data, together with previously published observations [93], are indicative of Golgi
527 bodies with multiple anterograde and retrograde pathways entering and exiting the organelle
528 present in all Preaxostyla species.

529 We did observe two clear differences in the sets of Golgi-associated proteins between the stacked
530 and unstacked Golgi-possessing organisms. Firstly, *P. pyriformis* encodes seven of the eight
531 Conserved Oligomeric Golgi (COG) complex proteins, while only a sparse representation of the
532 COG complex was seen in the oxymonads. Secondly, the golgin CASP was found in both
533 *P. pyriformis* and *T. marina*, but in none of the oxymonad genomes. The same was true for Golgin
534 84. This marks the first report of CASP or Golgin 84 from a metamonad [86] suggesting
535 independent losses of these proteins in the Oxymonadida, Parabasalia, and Fornicata lineages.
536 While caution is warranted when reporting the absence of any given single protein from any given
537 genome, our observations do show a greater number of encoded Golgi-structure implicated proteins
538 in the stacked-Golgi possessing lineages than in the oxymonads (4, 7 vs 1, 4, 3 respectively; Fig 4).
539 Though expression levels would need to be taken into account, this observation is nonetheless
540 consistent with the cisternal adhesion model [85], i.e., that it is the amount of adhesive golgin-type
541 proteins that regulate stacking rather than the identity of any given Golgi-stacking protein [86].

542 **Conclusions**

543 In this manuscript we report thorough searches for mitochondrion-associated proteins, which failed
544 to uncover any convincing candidates in the three investigated oxymonads but corroborate the
545 presence of a unique MRO type in *T. marina* and *P. pyriformis*. This shows that the absence of
546 mitochondria is not a unique feature of a single species, *M. exilis*, but applies to a wider range of
547 oxymonads, putatively the whole group. This fact moves this unique loss back to at least 100 MYA,
548 when oxymonads had been already diversified [94], and shows that a eukaryotic lineage without
549 mitochondria can thrive for a long time and undergo pronounced morphological evolution, as is
550 apparent from the range of shapes and specialized cellular structures exhibited by extant
551 oxymonads [10]. We also noticed that the loss of mitochondrion has not greatly affected the counts

552 of Fe-S cluster-containing proteins but led to a decrease in the usage of 2Fe-2S cluster types. On
553 the other hand, it might relate to the loss of large hydrogenases in oxymonads and the simplification
554 of their amino acid metabolism, which lacks the glycine cleavage system, a connection to one
555 carbon pool. The latter is considered the only essential function of MRO in *P. pyriformis* [17] and
556 its removal was probably the last step towards amitochondriality.

557 We also identified differences in inventories of membrane transporters between free-living
558 *P. pyriformis* and *T. marina* and oxymonads which we ascribe to the transition from the free-living
559 to the endobiotic lifestyle at the origin of oxymonads. Finally, proteins involved in the formation
560 and regulation of the Golgi structure have a patchy distribution and show a trend towards loss in
561 oxymonads, which is consistent with the lack of ultrastructural evidence for the presence of
562 a stacked Golgi in oxymonads, but also with an emerging cell biological model for how Golgi
563 maintain their hallmark morphology of stacked cisternae [85].

564 Materials and methods

565 Cell culture, DNA and RNA isolation

566 Monoeukaryotic, xenic culture of *P. pyriformis* (strain RCP-MX, ATCC 50935) was maintained
567 in the Sonneborn's Paramecium medium ATCC 802 at room temperature by serial transfer of one
568 ml of well-grown culture (approximately 5×10^4 cells/ml) into a 15 ml test tube containing 10 ml of
569 fresh, bacterized medium every week. The medium was bacterized 24 hours before the transfer.
570 *B. nauphoetae* strain NAU3 [21] was cultured in a similar way as described above but using
571 a modified TYSGM media [95].

572 For DNA isolation, 15 liters of *P. pyriformis* and 32 liters of *B. nauphoetae* culture were used. To
573 remove most of the bacterial contamination, the cells were filtered as described previously [7].

574 After filtration, the cells were collected at 1200×g for 10 min at four ºC. The DNA was isolated
575 using two different kits. The gDNA samples for PacBio, Illumina HiSeq, and Illumina MiSeq
576 sequencing were isolated using the Qiagen DNeasy Blood & Tissue Kit (Qiagen). The isolated
577 gDNA was further ethanol-precipitated to increase the concentration and remove any contaminants.
578 For Nanopore sequencing DNA was isolated using Qiagen MagAttract HMW DNA Kit (Qiagen)
579 according to the manufacturer's protocol.

580 RNA for Illumina transcriptome sequencing of *P. pyriformis* was isolated from 10 liters of a well-
581 grown culture using TRI reagent (Sigma-Aldrich). Eukaryotic mRNA was selected from total RNA
582 using Dynabeads Oligo(dT) beads (Thermo Fisher Scientific). cDNA was synthesized using the
583 SMARTer PCR cDNA Synthesis Kit (Takara Bio Group) and sequenced using the Illumina HiSeq
584 2000 sequencer at the Beijing Genomics Institute (BGI; Shenzhen, People's Republic of China).

585 For RNA isolation of *B. nauphoetae* we used 500 ml of a well-grown culture. Prior to RNA
586 isolation, the culture was filtered as described previously [7], and the cells were harvested by
587 centrifugation at 1200×g for 10 min at four ºC. The total RNA was isolated using TRI reagent
588 (Sigma-Aldrich) according to the manufacturer's protocol. From the total RNA, mRNA was
589 isolated using two rounds of Dynabeads Oligo(dT) beads (Thermo Fisher Scientific) according to
590 the manufacturer's protocol. The purified mRNA was used for *de novo* whole transcriptome
591 sequencing performed at the Beijing Genomics Institute (BGI; Shenzhen, People's Republic of
592 China).

593 **Library preparation, Illumina, and Nanopore sequencing**

594 For *P. pyriformis* PacBio sequencing was performed at SEQme s.r.o. (Dobříš, Czech Republic)
595 using a PacBio RSII sequencer, whereas Illumina sequencing was performed using Illumina HiSeq

596 and MiSeq sequencers at the Institute of Molecular Genetics of the ASCR, v. v. i. (Prague, Czech
597 Republic). For *B. nauphoetae*, one pair-end and two mate-pair libraries were prepared and
598 sequenced on Illumina MIseq PE 2x300bp at Beijing Genomics Institute (BGI; Shenzhen, People's
599 Republic of China).

600 Libraries for Nanopore sequencing were prepared from four µg of gDNA for each library. DNA
601 was sheared at ~20kbp using Covaris g-TUBES (Covaris Ltd, UK) and the library was prepared
602 using the ligation sequencing kit from Oxford Nanopore Technologies (SQK-LSK108) according
603 to the manufacturer's protocol. The prepared libraries were loaded onto a R9.4 Spot-On Flow cell
604 (FLO-MIN106) and sequencing was performed on a MinION Mk1B machine for 48 hours using
605 MinKNOW 2.0 software with live base calling enabled. In total we prepared four libraries and used
606 four flow-cells for sequencing, two for *P. pyriformis,* and two for *B. nauphoetae.*

607 **Genome assembly binning and decontamination**

608 The quality of sequencing data was assessed with FastQC (Babraham Bioinformatics, USA). For
609 the Illumina data, adapter and quality trimming were performed using Trimmomatic 0.36 [96], with
610 a quality threshold of 15. For the Nanopore data, trimming and removal of chimeric reads were
611 performed using Porechop v0.2.3 (github.com/rrwick/Porechop).

612 The initial assembly of the genomes was made only with the Nanopore and PacBio reads using
613 Canu v1.7.1 assembler [97], with corMinCoverage and corOutCoverage set to zero and 100,000
614 respectively. After assembly, the data was binned using tetraESOM [98]. The resulting eukaryotic
615 bins were also checked using a combination of BLASTn and a scoring strategy based on the identity
616 and coverage of the scaffold as described in Treitli et al. [99]. After binning, the resulting genomic
617 bins were polished in two phases. In the first phase, the scaffolds were polished with Nanopolish

618 [100] using the raw reads generated by Nanopore. In the second phase, the resulting scaffolds
619 generated by Nanopolish were further corrected using Illumina short reads with Pilon v1.21 [101].
620 Finally, the genome assembly of *P. pyriformis* was further scaffolded with raw RNA-seq reads
621 using Rascaf [102].

622 **Repeat masking, gene prediction, and annotation of the genomes**

623 Repetitive elements in the genomic assembly were identified using RepeatModeler v1.0.11 [103],
624 and only repeats that are members of known repeat families were used for masking the genome
625 assemblies prior to gene prediction. For the *P. pyriformis* and *B. nauphoetae*, we used Augustus
626 3.2.3 for gene prediction [104]. For *de novo* prediction of genes, Augustus was first re-trained using
627 a set of gene models manually curated by considering information from mapped transcriptomic
628 sequences and sequence conservation with homologous protein-coding genes. In the next step,
629 intron hints were generated from the RNAseq data and gene prediction was performed on repeat-
630 masked genomes using Augustus. Next, transcriptome assemblies were mapped to the genomes
631 using PASA [105] and the resulting assembled transcripts were used as evidence for gene model
632 polishing with EVM [106]. The genome completeness for each genome was estimated using
633 BUSCO v3 with the Eukaryota odb9 dataset and the genome completeness was estimated on the
634 sets of EVM-polished protein sequences as the input. Reference-independent genome
635 completeness estimation was performed using Merqury [19] with the Illumina decontaminated
636 reads. To avoid bias in the results, the read decontamination was performed by removing only those
637 reads that mapped to the contaminants identified during genome decontamination.

638 Automatic functional annotation of the predicted genes was performed using the KEGG Automatic
639 Annotation Server [107], in parallel to similarity searches against NCBI nr protein database using
640 BLASTp. If both gave functional annotation, BLAST was preferred if the e-value was lower than

641 10^{-30}. Otherwise KEGG was used. Targeted analyses of genes and gene families of specific interest
642 were performed by manual searches of the predicted proteomes using BLASTp and HMMER
643 [108], and complemented by tBLASTn searches of the genome and transcriptome assemblies to
644 check for the presence of individual genes of interest that were potentially missed in the predicted
645 protein sets (single digits of cases per set). Gene models were manually refined for genes of interest
646 when necessary and possible. The annotated genomes were deposited in NCBI under accession
647 number JAPMOS000000000 for *P. pyriformis* and JARBJD000000000 for *B. nauphoetae*.

648 **Orthology grouping**

649 We combined the gene inventories of five Preaxostyla species (the two genomes presented here,
650 the *M. exilis* genome GiardiaDB-46_MexilisPA203 in GiardiaDB release 46, the *S. strix* genome
651 under NCBI BioProject PRJNA524138, and the *T. marina* transcriptome-derived predicted
652 proteome in EukProt EP00771, [109]) with 14 other metamonads for which the genome or
653 transcriptome drafts were available when the study was initiated (S3 File, Sheet 1). To optimize
654 the inflation parameter value of OrthoMCL, we performed multiple clustering runs with different
655 inflation parameter values in the range 1.01 to 30.0 and calculated the number of OGs containing
656 genes from all Preaxostyla but no other taxa and from all oxymonads but no other taxa. We chose
657 to proceed with the value of inflation parameter=4, because under this setting the sum of these two
658 numbers was the highest, so the strength of the clustering should be optimal for our purpose. Under
659 this setting, the complete set of proteins from the 19 species (337,300 items) was assigned to 37,923
660 groups of genes or singletons (OGs) (S3 File, Sheet 2). Proteins belonging to these OGs were
661 automatically annotated using BLASTp searches against the NCBI nr protein database to acquire
662 functional annotation (S3 File, Sheet 3). Venn diagrams were generated using InteractiVenn [110].

663 **Search for mitochondrial proteins**

664 The comprehensive search for putative mitochondrial protein was performed for all five
665 Preaxostyla species, including the previously analyzed *M. exilis* [7] as a control. The general design
666 of the search followed the previously described methodology [7]. Briefly, a custom mitochondrial
667 protein sequence database was compiled using the MitoMiner v4.0 database [22,23] as the core
668 and supplemented with MROs proteins from sixteen different organisms [5,50,51,63,111–116],
669 herein referred to as MitoMiner. Redundant homologues (90% similarity threshold) were removed
670 from the database using CD-HIT. The resulting non-redundant database contained 6,979 proteins.

671 Most searches were divided in three phases. 1) hits generated by HMM searches, predictions
672 mitochondrial targeting sequence, transmembrane domains of TA proteins or mitochondrial β-
673 barrel outer membrane proteins, were in (2) narrowed down to candidates, proteins with hits in the
674 MitoMiner database. 3) All candidates were BLAST-searched against the NCBI nr database and
675 the best hits with the descriptions not including the terms 'low quality protein', 'hypothetical',
676 'unknown', etc. were kept. Gene Ontology categories were assigned using InterProScan-5.36-75.0.
677 If the annotations received from BLAST or InterProScan corresponded to the originally suggested
678 reliably mitochondrial function, the candidates were considered as mitochondrial proteins.

679 HMM searches using HMMER 3.1b2 and profile HMMs previously employed by Karnkowska et
680 al. [7] were performed to specifically identify proteins involved in mitochondrial protein import
681 and translocation, as these were shown to be often divergent [51]. Mitochondrial targeting signals
682 were detected using TargetP v1.1 [117] and MitoFates v1.1 [118]. Both programs indicate
683 a probability of mitochondrial localization of the protein. Hits with the probability of mitochondrial
684 localization indicated to be >0.5 by both programs were considered for manual verification. To
685 find tail-anchored proteins, transmembrane domains (TMDs) were predicted using TMHMM2.0

686 [119] for all analyzed proteins. Hits with a TMD within 32 amino acid residues from the C-terminus
687 were kept for verification. The mitochondrial β-barrel outer membrane proteins (MBOMPs) search
688 has been conducted using the pipeline described by Imai et al. [120]. The pipeline firstly identifies
689 a β-signal ($P_oxGh_yxH_yxH_y$ motif), required for the insertion into the membrane, in the C-terminus
690 of the query protein. Subsequently, the secondary structure of the stretch of 300 amino acid residues
691 preceding the β-signal is analyzed using PSIPRED [121] to check for a typical β-structure.
692 Significant hits, with at least 25% of the sequence predicted to form β-strands, no more than 10%
693 assumed by an α-helical structure, and no more than 50% of the eight residues of the β-signal
694 predicted as an α-helical structure, were analyzed further.

695 On the top of the three-phase searches, we have also performed one extensive but low specificity
696 homology search in which reciprocal BLAST analysis using the MitoMiner database was
697 performed for each predicted proteome of Preaxostyla species with an e-value threshold of 0.001.
698 Functional annotation of the reciprocal hits was assessed by NCBI BLAST and items were
699 inspected for cases of reliable mitochondrial proteins.

700 ***Trypanosoma brucei* mitoproteome-guided comparative analyses**

701 Predicted proteomes of *T. marina*, *P. pyriformis*, *S. strix*, *B. nauphoetae,* and *M. exilis* were
702 individually reverse BLAST-searched against the proteome of *T. brucei* (downloaded from
703 Tritrypdb.org; November 2019; [122]). Only reciprocal best BLAST hits that were identified in
704 any of the previously published mitochondrial proteomes of *T. brucei* [37,39] were subjected to
705 further phylogenetic analysis. For each such protein, the data set for the tree construction was
706 composed of hits from a custom BLAST database of selected protist proteomes (downloaded from
707 UniProt, November 2019; [123]). Protein sequence sets were automatically aligned with MAFFT
708 v7.453 using the L-INS-i refinement and a maximum of 1,000 iterations, followed by trimming of

709 sites with >70% gaps. ML trees (S5 File) were inferred by IQ-TREE v 1.6.12 using the Posterior
710 Mean Site Frequency (PMSF) empirical model with the ultrafast bootstrapping strategy (1,000
711 replicates) and a LG4X guide tree [124]. Subcellular targeting of all proteins in the tree was
712 predicted by using TargetP-1.1; the presence of a signal peptide, a chloroplast targeting peptide or
713 a mitochondrial targeting peptide in the respective proteins is marked by the letters S, C, or M,
714 respectively, at the very beginning of the sequence names.

715 **Prediction of proteins containing Fe-S clusters**

716 Fe-S cluster containing proteins were predicted with MetalPredator webserver [125]. Predicted
717 proteins were functionally annotated by BLAST searches against the NCBI nr database and by
718 InterProScan against the InterPro database [126]. KEGG categories were assigned by
719 GhostKOALA searches against the KEGG database [127]. Orthologous groups were created with
720 the OrthoFinder 2 software [128] and the Venn diagram of OG sharing among Preaxostyla was
721 visualized using InteractiVenn.

722 **Search for Peroxins and enzymes for the heme synthesis**

723 The peroxins and the proteins involved in heme biosynthesis were identified by BLASTp searches.
724 All BLASTp hits with an e-value of less than 0.1 were further analyzed by reciprocal BLASTp and
725 HHpred [129].

726 **Single gene phylogenies**

727 The phylogenies of the genes of interest were analyzed individually using the methodology
728 described below. Eukaryotic homologues of the Preaxostyla genes were gathered by taxonomically
729 constrained iterative BLAST search against publicly available sequence databases in order to
730 sample as broad eukaryotic diversity as possible. In the cases of overrepresented taxa of low interest

731 (e.g. Metazoa, land plants), only a small number of representative sequences were selected
732 arbitrarily. In order to detect potential LGT from prokaryotes while keeping the number of included
733 sequences manageable, prokaryotic homologues were gathered by a BLASTp search with each
734 eukaryotic sequence against the NCBI nr database with an e-value cutoff of 10^{-10} and max. 10 target
735 sequences. The sequences were aligned using MAFFT and automatically trimmed using trimAl
736 v1.2 [130]. Phylogenetic analyses were performed simultaneously using IQ-TREE v2.0.5 [124]
737 and RAxML-HPC2 on v8.2.12 [131] with the LG4X model on the Cyberinfrastructure for the
738 Phylogenetic Research (CIPRES) Science Gateway [132]. Substitution models were inferred using
739 IQ-TREE TESTNEW function for IQ-TREE.

740 **Phylogenetic analysis of Golgi-related proteins**

741 Comparative genomics was carried out using HMM searches. Pan-eukaryotic query sequences
742 analyzed and curated for previous pan-eukaryotic vesicle coat, multisubunit tethering complexes,
743 and golgins were used to build profile HMMs. Query sequences were obtained from the
744 supplementary material of previous papers dealing specifically with Adaptins and COPI [133],
745 multisubunit tethering complexes [134], and golgins [86]. Individual components and proteins
746 from each sub-complex were aligned using MUSCLE v.3.8.31 and the resulting alignment files
747 were used to generate HMM matrices using the HMMBUILD option available through the
748 HMMER package. HMMER searches were carried out in the predicted proteomes of *P. pyriformis*,
749 *B. nauphoetae*, and *S. strix*, whereas for *T. marina* the transcriptome assembly was first translated
750 in all six open reading frames using the *ab initio* gene prediction program GeneMarkS-T using the
751 default parameters [135] and the longest resulting predicted protein sequences were used for the
752 searches. Forward hits meeting an e-value cutoff of 0.05 were subject to reciprocal BLASTp
753 analyses against the *Homo sapiens* and *M. exilis* predicted proteomes as well as the NCBI nr

754 database. Any absent components were also subject to additional tBLASTn searches in the
755 nucleotide scaffolds. Hits were deemed positive if both forward hits and at least two of three
756 reciprocal BLAST results retrieved the correct orthologue with an e-value cutoff of 0.05.
757 Paralogous gene families were subject to further phylogenetic analyses.

758 Phylogenetic analyses were undertaken for the large, medium, and small subunits from identified
759 AP1-4 and CopI families, as well as Syntaxin16 and Syntaxin5. Resolved backbone alignments
760 from the dataset curated for Karnkowska et al. [8] were used and sequences from *T. marina*,
761 *P. pyriformis*, *B. nauphoetae*, and *S. strix* were iteratively aligned with the backbone alignment
762 using the profile option available through MUSCLE v3.8.31 [136]. All alignments were
763 subsequently inspected and manually trimmed using Mesquite v. 3.5 (mesquiteproject.org) to
764 remove heterogeneous regions lacking obvious homology and partial or misaligned sequences.

765 Maximum likelihood analyses were carried out using RAxML-HPC2 on XSEDE v.8.2.10 for non-
766 parametric bootstrap replicates [137]. The best protein matrix model for RAxML was tested using
767 ProtTest v.3.4.2 [138], set to account for Gamma rate variation (+G), invariant sites (+I), and
768 observed frequency of amino acids (+F) with default tree and a consensus tree was obtained using
769 the Consense package, available through the Phylip v.3.66 [139].

770 Bayesian inference was carried out using MRBAYES on XSEDE v3.2.6 [140]. Parameters
771 specified included 10 million Markov Chain Monte Carlo generations under a mixed amino acid
772 model with the number of gamma rate categories set a 4. The sampling frequency was set to occur
773 every 1000 generations with a burn-in of 0.25. Tree convergence was ensured with the average
774 standard deviation of split frequency values below 0.01. Both RAxML and MRBAYES analyses
775 were performed on the CIPRES webserver. RAxML bootstrap values as well as Bayesian posterior

776 probabilities were overlaid on the best Bayes topology with combined values of >50 and >0.80,

777 respectively, indicating branch support. All alignments are available upon request.

Financial disclosure

This project has received funding from the European Research Council (ERC) under the European Union's Horizon 2020 research and innovation programme (grant agreement No. 771592) and the Centre for research of pathogenicity and virulence of parasites (registration no. CZ.02.1.01/0.0/0.0/16_019/0000759). Computational resources were supplied by the project "e-Infrastruktura CZ" (e-INFRA LM2018140) provided within the program Projects of Large Research, Development and Innovations Infrastructures. Research in Karnkowska lab is supported by EMBO Installation Grant 4150 and Ministry of Education and Science, Poland and the Interdisciplinary Centre for Mathematical and Computational Modelling (ICM) University of Warsaw under computational allocation no. G 72-16. Research in the Dacks Lab is supported by grants from the Natural Sciences and Research Council of Canada (RES0021028, RES0043758, and RES0046091) and SVP received salary support through Alberta Innovates Graduate Studentship (Doctoral) and Canadian Institutes of Health Research Canada Graduate Scholarships. ME was supported by the Czech Science Foundation project 22-29633S. Funders had no role in the design of the study and collection, analysis, and interpretation of data or in writing the manuscript. LVFN, SCT, JP, VV, OB, PS, and VH received a salary from ERC (771592). ME received a salary from the Czech Science Foundation (22-29633S).

795 # References

796 1. Roger AJ, Muñoz-Gómez SA, Kamikawa R. The origin and diversification of mitochondria.
797 Curr Biol. 2017;27: R1177–R1192. doi:10.1016/j.cub.2017.09.015

798 2. Müller M, Mentel M, van Hellemond JJ, Henze K, Woehle C, Gould SB, et al. Biochemistry
799 and evolution of anaerobic energy metabolism in eukaryotes. Microbiol Mol Biol Rev.
800 2012;76: 444–495. doi:10.1128/MMBR.05024-11

801 3. Stairs CW, Leger MM, Roger AJ. Diversity and origins of anaerobic metabolism in
802 mitochondria and related organelles. Philos Trans R Soc B. 2015;370: 20140326.
803 doi:10.1098/rstb.2014.0326

804 4. Klinger CM, Karnkowska A, Herman EK, Hampl V, Dacks JB. Phylogeny and evolution. In:
805 Walochnik J, Duchêne M, editors. Molecular parasitology: protozoan parasites and their
806 molecules. Vienna: Springer; 2016. pp. 383–408. doi:10.1007/978-3-7091-1416-2_12

807 5. Leger MM, Kolisko M, Kamikawa R, Stairs CW, Kume K, Čepička I, et al. Organelles that
808 illuminate the origins of *Trichomonas* hydrogenosomes and *Giardia* mitosomes. Nat Ecol
809 Evol. 2017;1: 0092. doi:10.1038/s41559-017-0092

810 6. Onuț-Brännström I, Stairs CW, Campos KIA, Thorén MH, Ettema TJG, Keeling PJ, et al. A
811 mitosome with distinct metabolism in the uncultured protist parasite *Paramikrocytos canceri*
812 (Rhizaria, Ascetosporea). Genome Biol Evol. 2023;15: evad022. doi:10.1093/gbe/evad022

813 7. Karnkowska A, Vacek V, Zubáčová Z, Treitli SC, Petrželková R, Eme L, et al. A eukaryote
814 without a mitochondrial organelle. Curr Biol. 2016;26: 1274–1284.
815 doi:10.1016/j.cub.2016.03.053

816 8. Karnkowska A, Treitli SC, Brzoň O, Novák L, Vacek V, Soukal P, et al. The oxymonad
817 genome displays canonical eukaryotic complexity in the absence of a mitochondrion. Mol
818 Biol Evol. 2019;36: 2292–2312. doi:10.1093/molbev/msz147

819 9. Treitli SC, Peña-Diaz P, Hałakuc P, Karnkowska A, Hampl V. High quality genome
820 assembly of the amitochondriate eukaryote *Monocercomonoides exilis*. Microb Genom.
821 2021;7: 000745. doi:10.1099/mgen.0.000745

822 10. Hampl V. Preaxostyla. In: Archibald JM, Simpson AGB, Slamovits CH, editors. Handbook
823 of the Protists. Cham: Springer International Publishing; 2017. pp. 1139–1174.
824 doi:10.1007/978-3-319-28149-0_8

825 11. Yazaki E, Kume K, Shiratori T, Eglit Y, Tanifuji G, Harada R, et al. Barthelonids represent a
826 deep-branching metamonad clade with mitochondrion-related organelles predicted to
827 generate no ATP. Proc Biol Sci. 2020;287: 20201538. doi:10.1098/rspb.2020.1538

828 12. Williams SK, Hultqvist JJ, Eglit Y, Salas-Leiva DE, Curtis B, Orr R, et al. Extreme
829 mitochondrial reduction in a novel group of free-living metamonads. bioRxiv; 2023. p.
830 2023.05.03.539051. doi:10.1101/2023.05.03.539051

831 13. Stairs CW, Táborský P, Salomaki ED, Kolisko M, Pánek T, Eme L, et al. Anaeramoebae are
832 a divergent lineage of eukaryotes that shed light on the transition from anaerobic
833 mitochondria to hydrogenosomes. Curr Biol. 2021;31: 5605-5612.e5.
834 doi:10.1016/j.cub.2021.10.010

835 14. Zhang Q, Táborský P, Silberman JD, Pánek T, Čepička I, Simpson AGB. Marine isolates of
836 *Trimastix marina* form a plesiomorphic deep-branching lineage within Preaxostyla, separate
837 from other known trimastigids (*Paratrimastix* n. gen.). Protist. 2015;166: 468–491.
838 doi:10.1016/j.protis.2015.07.003

839 15. Hampl V, Silberman JD, Stechmann A, Diaz-Triviño S, Johnson PJ, Roger AJ. Genetic
840 Evidence for a mitochondriate ancestry in the 'amitochondriate' flagellate *Trimastix*
841 *pyriformis*. PLoS One. 2008;3: e1383. doi:10.1371/journal.pone.0001383

842 16. Zubáčová Z, Novák L, Bublíková J, Vacek V, Fousek J, Rídl J, et al. The mitochondrion-like
843 organelle of *Trimastix pyriformis* contains the complete glycine cleavage system. PLoS One.
844 2013;8: e55417. doi:10.1371/journal.pone.0055417

845 17. Zítek J, Füssy Z, Treitli SC, Peña-Diaz P, Vaitová Z, Zavadska D, et al. Reduced
846 mitochondria provide an essential function for the cytosolic methionine cycle. Curr Biol.
847 2022;32: 5057-5068.e5. doi:10.1016/j.cub.2022.10.028

848 18. Simão FA, Waterhouse RM, Ioannidis P, Kriventseva EV, Zdobnov EM. BUSCO: assessing
849 genome assembly and annotation completeness with single-copy orthologs. Bioinformatics.
850 2015;31: 3210–3212. doi:10.1093/bioinformatics/btv351

851 19. Rhie A, Walenz BP, Koren S, Phillippy AM. Merqury: reference-free quality, completeness,
852 and phasing assessment for genome assemblies. Genome Biol. 2020;21: 245.
853 doi:10.1186/s13059-020-02134-9

854 20. Wilson DN, Doudna Cate JH. The structure and function of the eukaryotic ribosome. Cold
855 Spring Harb Perspect Biol. 2012;4: a011536. doi:10.1101/cshperspect.a011536

856 21. Treitli SC, Kotyk M, Yubuki N, Jirounková E, Vlasáková J, Smejkalová P, et al. Molecular
857 and morphological diversity of the oxymonad genera *Monocercomonoides* and *Blattamonas*
858 gen. nov. Protist. 2018;169: 744–783. doi:10.1016/j.protis.2018.06.005

859 22. Smith AC, Blackshaw JA, Robinson AJ. MitoMiner: a data warehouse for mitochondrial
860 proteomics data. Nucleic Acids Res. 2012;40: D1160-1167. doi:10.1093/nar/gkr1101

861 23. Smith AC, Robinson AJ. MitoMiner v4.0: an updated database of mitochondrial localization
862 evidence, phenotypes and diseases. Nucleic Acids Res. 2019;47: D1225–D1228.
863 doi:10.1093/nar/gky1072

24. Pfanner N, Warscheid B, Wiedemann N. Mitochondrial proteins: from biogenesis to functional networks. Nat Rev Mol Cell Biol. 2019;20: 267–284. doi:10.1038/s41580-018-0092-0

25. Eberhardt EL, Ludlam AV, Tan Z, Cianfrocco MA. Miro: A molecular switch at the center of mitochondrial regulation. Protein Sci. 2020;29: 1269–1284. doi:10.1002/pro.3839

26. Vlahou G, Eliáš M, von Kleist-Retzow J-C, Wiesner RJ, Rivero F. The Ras related GTPase Miro is not required for mitochondrial transport in *Dictyostelium discoideum*. Eur J Cell Biol. 2011;90: 342–355. doi:10.1016/j.ejcb.2010.10.012

27. Gentekaki E, Curtis BA, Stairs CW, Klimeš V, Eliáš M, Salas-Leiva DE, et al. Extreme genome diversity in the hyper-prevalent parasitic eukaryote *Blastocystis*. PLoS Biol. 2017;15: e2003769. doi:10.1371/journal.pbio.2003769

28. Zítek J, King MS, Peña-Diaz P, Pyrihová E, King AC, Kunji ERS, et al. The free-living flagellate *Paratrimastix pyriformis* uses a distinct mitochondrial carrier to balance adenine nucleotide pools. Arch Biochem Biophys. 2023;742: 109638. doi:10.1016/j.abb.2023.109638

29. Tsaousis AD, Kunji ERS, Goldberg AV, Lucocq JM, Hirt RP, Embley TM. A novel route for ATP acquisition by the remnant mitochondria of *Encephalitozoon cuniculi*. Nature. 2008;453: 553–556. doi:10.1038/nature06903

30. Dolezal P, Likic V, Tachezy J, Lithgow T. Evolution of the molecular machines for protein import into mitochondria. Science. 2006;313: 314–318. doi:10.1126/science.1127895

31. Lucattini R, Likic VA, Lithgow T. Bacterial proteins predisposed for targeting to mitochondria. Mol Biol Evol. 2004;21: 652–658. doi:10.1093/molbev/msh058

32. Fang Y-K, Vaitová Z, Hampl V. A mitochondrion-free eukaryote contains proteins capable of import into an exogenous mitochondrion-related organelle. Open Biol. 2023;13: 220238. doi:10.1098/rsob.220238

33. Borgese N, Brambillasca S, Colombo S. How tails guide tail-anchored proteins to their destinations. Curr Opin Cell Biol. 2007;19: 368–375. doi:10.1016/j.ceb.2007.04.019

34. Denic V. A portrait of the GET pathway as a surprisingly complicated young man. Trends Biochem Sci. 2012;37: 411–417. doi:10.1016/j.tibs.2012.07.004

35. Rada P, Makki A, Žárský V, Tachezy J. Targeting of tail-anchored proteins to *Trichomonas vaginalis* hydrogenosomes. Mol Microbiol. 2019;111: 588–603. doi:10.1111/mmi.14175

36. van der Bliek AM, Shen Q, Kawajiri S. Mechanisms of mitochondrial fission and fusion. Cold Spring Harb Perspect Biol. 2013;5: a011072. doi:10.1101/cshperspect.a011072

37. Panigrahi AK, Ogata Y, Zíková A, Anupama A, Dalley RA, Acestor N, et al. A comprehensive analysis of *Trypanosoma brucei* mitochondrial proteome. Proteomics. 2009;9: 434–450. doi:10.1002/pmic.200800477

899 38. Dean S, Sunter JD, Wheeler RJ. TrypTag.org: A trypanosome genome-wide protein
900 localisation resource. Trends Parasitol. 2017;33: 80–82. doi:10.1016/j.pt.2016.10.009

901 39. Peikert CD, Mani J, Morgenstern M, Käser S, Knapp B, Wenger C, et al. Charting organellar
902 importomes by quantitative mass spectrometry. Nat Commun. 2017;8: 15272.
903 doi:10.1038/ncomms15272

904 40. Pyrih J, Hammond M, Alves A, Dean S, Sunter JD, Wheeler RJ, et al. Comprehensive sub-
905 mitochondrial protein map of the parasitic protist *Trypanosoma brucei* defines critical
906 features of organellar biology. Cell Rep. 2023;42: 113083. doi:10.1016/j.celrep.2023.113083

907 41. Tice AK, Žihala D, Pánek T, Jones RE, Salomaki ED, Nenarokov S, et al. PhyloFisher: A
908 phylogenomic package for resolving eukaryotic relationships. PLoS Biol. 2021;19:
909 e3001365. doi:10.1371/journal.pbio.3001365

910 42. Duschak VG, Cazzulo JJ. Subcellular localization of glutamate dehydrogenases and alanine
911 aminotransferase in epimastigotes of *Trypanosoma cruzi*. FEMS Microbiol Lett. 1991;67:
912 131–135. doi:10.1016/0378-1097(91)90343-9

913 43. Saas J, Ziegelbauer K, von Haeseler A, Fast B, Boshart M. A developmentally regulated
914 aconitase related to iron-regulatory protein-1 is localized in the cytoplasm and in the
915 mitochondrion of *Trypanosoma brucei*. J Biol Chem. 2000;275: 2745–2755.
916 doi:10.1074/jbc.275.4.2745

917 44. Yagi T, Shounaka M, Yamamoto S. Distribution of aspartate aminotrasnsferase activity in
918 yeasts, and purification and characterization of mitochondrial and cytosolic isoenzymes from
919 *Rhodotorula marina*. J Biochem. 1990;107: 151–159.
920 doi:10.1093/oxfordjournals.jbchem.a123000

921 45. Peña-Diaz J, Montalvetti A, Flores C-L, Constán A, Hurtado-Guerrero R, De Souza W, et al.
922 Mitochondrial localization of the mevalonate pathway enzyme 3-Hydroxy-3-methyl-glutaryl-
923 CoA reductase in the Trypanosomatidae. Mol Biol Cell. 2004;15: 1356–1363.
924 doi:10.1091/mbc.e03-10-0720

925 46. Lindmark DG, Müller M. Hydrogenosome, a cytoplasmic organelle of the anaerobic
926 flagellate *Tritrichomonas foetus*, and its role in pyruvate metabolism. J Biol Chem. 1973;248:
927 7724–7728. doi:10.1016/S0021-9258(19)43249-3

928 47. Williams K, Lowe PN, Leadlay PF. Purification and characterization of pyruvate: ferredoxin
929 oxidoreductase from the anaerobic protozoon *Trichomonas vaginalis*. Biochem J. 1987;246:
930 529–536. doi:10.1042/bj2460529

931 48. Payne MJ, Chapman A, Cammack R. Evidence for an [Fe]-type hydrogenase in the parasitic
932 protozoan *Trichomonas vaginalis*. FEBS Lett. 1993;317: 101–104. doi:10.1016/0014-
933 5793(93)81500-y

934 49. Tachezy J, Doležal P. Iron–sulfur proteins and iron–sulfur Cluster assembly in organisms
935 with hydrogenosomes and mitosomes. In: Martin WF, Müller M, editors. Origin of

936 Mitochondria and Hydrogenosomes. Berlin, Heidelberg: Springer; 2007. pp. 105–133.
937 doi:10.1007/978-3-540-38502-8_6

938 50. Stairs CW, Eme L, Brown MW, Mutsaers C, Susko E, Dellaire G, et al. A SUF Fe-S cluster
939 biogenesis system in the mitochondrion-related organelles of the anaerobic protist *Pygsuia*.
940 Curr Biol. 2014;24: 1176–1186. doi:10.1016/j.cub.2014.04.033

941 51. Leger MM, Eme L, Hug LA, Roger AJ. Novel hydrogenosomes in the microaerophilic
942 jakobid *Stygiella incarcerata*. Mol Biol Evol. 2016;33: 2318–2336.
943 doi:10.1093/molbev/msw103

944 52. Treitli SC, Hanousková P, Beneš V, Brune A, Čepička I, Hampl V. Hydrogenotrophic
945 methanogenesis is the key process in the obligately syntrophic consortium of the anaerobic
946 ameba *Pelomyxa schiedti*. ISME J. 2023;17: 1884–1894. doi:10.1038/s41396-023-01499-6

947 53. Greening C, Biswas A, Carere CR, Jackson CJ, Taylor MC, Stott MB, et al. Genomic and
948 metagenomic surveys of hydrogenase distribution indicate H2 is a widely utilised energy
949 source for microbial growth and survival. ISME J. 2016;10: 761–777.
950 doi:10.1038/ismej.2015.153

951 54. Schut GJ, Adams MWW. The iron-hydrogenase of *Thermotoga maritima* utilizes ferredoxin
952 and NADH synergistically: a new perspective on anaerobic hydrogen production. J Bacteriol.
953 2009;191: 4451–4457. doi:10.1128/JB.01582-08

954 55. Vargová R, Hanousková P, Salamonová J, Žihala D, Silberman JD, Eliáš M, et al. Evidence
955 for an independent hydrogenosome-to-mitosome transition in the CL3 lineage of fornicates.
956 Front Microbiol. 2022;13: 866459. doi:10.3389/fmicb.2022.866459

957 56. Jerlström-Hultqvist J, Einarsson E, Xu F, Hjort K, Ek B, Steinhauf D, et al. Hydrogenosomes
958 in the diplomonad *Spironucleus salmonicida*. Nat Commun. 2013;4: 2493.
959 doi:10.1038/ncomms3493

960 57. Carlton JM, Hirt RP, Silva JC, Delcher AL, Schatz M, Zhao Q, et al. Draft genome sequence
961 of the sexually transmitted pathogen *Trichomonas vaginalis*. Science. 2007;315: 207–212.
962 doi:10.1126/science.1132894

963 58. Xu F, Jerlström-Hultqvist J, Einarsson E, Astvaldsson A, Svärd SG, Andersson JO. The
964 genome of *Spironucleus salmonicida* highlights a fish pathogen adapted to fluctuating
965 environments. PLoS Genet. 2014;10: e1004053. doi:10.1371/journal.pgen.1004053

966 59. Novák L, Zubáčová Z, Karnkowska A, Kolisko M, Hroudová M, Stairs CW, et al. Arginine
967 deiminase pathway enzymes: evolutionary history in metamonads and other eukaryotes.
968 BMC Evol Biol. 2016;16: 197. doi:10.1186/s12862-016-0771-4

969 60. Anderson IJ, Loftus BJ. *Entamoeba histolytica*: observations on metabolism based on the
970 genome sequence. Exp Parasitol. 2005;110: 173–177. doi:10.1016/j.exppara.2005.03.010

971 61. Ducker GS, Rabinowitz JD. One-carbon metabolism in health and disease. Cell Metab.
972 2017;25: 27–42. doi:10.1016/j.cmet.2016.08.009

973 62. Stipanuk MH. Metabolism of sulfur-containing amino acids. Annu Rev Nutr. 1986;6: 179–
974 209. doi:10.1146/annurev.nu.06.070186.001143

975 63. Nývltová E, Stairs CW, Hrdý I, Rídl J, Mach J, Pačes J, et al. Lateral gene transfer and gene
976 duplication played a key role in the evolution of *Mastigamoeba balamuthi* hydrogenosomes.
977 Mol Biol Evol. 2015;32: 1039–1055. doi:10.1093/molbev/msu408

978 64. Spalding MD, Prigge ST. Lipoic acid metabolism in microbial pathogens. Microbiol Mol
979 Biol Rev. 2010;74: 200–228. doi:10.1128/MMBR.00008-10

980 65. Babady NE, Pang Y-P, Elpeleg O, Isaya G. Cryptic proteolytic activity of dihydrolipoamide
981 dehydrogenase. Proc Natl Acad Sci U S A. 2007;104: 6158–6163.
982 doi:10.1073/pnas.0610618104

983 66. Petrat F, Paluch S, Dogruöz E, Dörfler P, Kirsch M, Korth H-G, et al. Reduction of Fe(III)
984 ions complexed to physiological ligands by lipoyl dehydrogenase and other flavoenzymes in
985 vitro: implications for an enzymatic reduction of Fe(III) ions of the labile iron pool. J Biol
986 Chem. 2003;278: 46403–46413. doi:10.1074/jbc.M305291200

987 67. Igamberdiev AU, Bykova NV, Ens W, Hill RD. Dihydrolipoamide dehydrogenase from
988 porcine heart catalyzes NADH-dependent scavenging of nitric oxide. FEBS Lett. 2004;568:
989 146–150. doi:10.1016/j.febslet.2004.05.024

990 68. Xia L, Björnstedt M, Nordman T, Eriksson LC, Olsson JM. Reduction of ubiquinone by
991 lipoamide dehydrogenase. An antioxidant regenerating pathway. Eur J Biochem. 2001;268:
992 1486–1490. doi:10.1046/j.1432-1327.2001.02013.x

993 69. Braymer JJ, Freibert SA, Rakwalska-Bange M, Lill R. Mechanistic concepts of iron-sulfur
994 protein biogenesis in Biology. Biochim Biophys Acta Mol Cell Res. 2021;1868: 118863.
995 doi:10.1016/j.bbamcr.2020.118863

996 70. Vacek V, Novák LVF, Treitli SC, Táborský P, Čepička I, Kolísko M, et al. Fe–S cluster
997 assembly in oxymonads and related protists. Mol Biol Evol. 2018;35: 2712–2718.
998 doi:10.1093/molbev/msy168

999 71. Peña-Diaz P, Braymer JJ, Vacek V, Zelená M, Lometto S, Hrdý I, et al. Characterisation of
1000 the SUF FeS cluster machinery in the amitochondriate eukaryote *Monocercomonoides exilis*.
1001 bioRxiv; 2023. p. 2023.03.30.534840. doi:10.1101/2023.03.30.534840

1002 72. Andreini C, Banci L, Rosato A. Exploiting bacterial operons to illuminate human iron-sulfur
1003 proteins. J Proteome Res. 2016;15: 1308–1322. doi:10.1021/acs.jproteome.6b00045

1004 73. Le T, Žárský V, Nývltová E, Rada P, Harant K, Vancová M, et al. Anaerobic peroxisomes in
1005 *Mastigamoeba balamuthi*. Proc Natl Acad Sci U S A. 2020;117: 2065–2075.
1006 doi:10.1073/pnas.1909755117

1007 74. Verner Z, Žárský V, Le T, Narayanasamy RK, Rada P, Rozbeský D, et al. Anaerobic
1008 peroxisomes in *Entamoeba histolytica* metabolize myo-inositol. PLoS Pathog. 2021;17:
1009 e1010041. doi:10.1371/journal.ppat.1010041

1010 75. Záhonová K, Treitli SC, Le T, Škodová-Sveráková I, Hanousková P, Čepička I, et al.
1011 Anaerobic derivates of mitochondria and peroxisomes in the free-living amoeba *Pelomyxa*
1012 *schiedti* revealed by single-cell genomics. BMC Biol. 2022;20: 56. doi:10.1186/s12915-022-
1013 01247-w

1014 76. Záhonová K, Low RS, Warren CJ, Cantoni D, Herman EK, Yiangou L, et al. Evolutionary
1015 analysis of cellular reduction and anaerobicity in the hyper-prevalent gut microbe
1016 *Blastocystis*. Curr Biol. 2023;33: 2449-2464.e8. doi:10.1016/j.cub.2023.05.025

1017 77. Kim PK, Hettema EH. Multiple pathways for protein transport to peroxisomes. J Mol Biol.
1018 2015;427: 1176–1190. doi:10.1016/j.jmb.2015.02.005

1019 78. Kořený L, Oborník M, Horáková E, Waller RF, Lukeš J. The convoluted history of haem
1020 biosynthesis. Biol Rev Camb Philos Soc. 2022;97: 141–162. doi:10.1111/brv.12794

1021 79. Nakjang S, Williams TA, Heinz E, Watson AK, Foster PG, Sendra KM, et al. Reduction and
1022 expansion in microsporidian genome evolution: new insights from comparative genomics.
1023 Genome Biol Evol. 2013;5: 2285–2303. doi:10.1093/gbe/evt184

1024 80. Harding T, Roger AJ, Simpson AGB. Adaptations to high salt in a halophilic protist:
1025 differential expression and gene acquisitions through duplications and gene transfers. Front
1026 Microbiol. 2017;8: 944. doi:10.3389/fmicb.2017.00944

1027 81. Lenassi M, Gostinčar C, Jackman S, Turk M, Sadowski I, Nislow C, et al. Whole genome
1028 duplication and enrichment of metal cation transporters revealed by de novo genome
1029 sequencing of extremely halotolerant black yeast *Hortaea werneckii*. PLoS One. 2013;8:
1030 e71328. doi:10.1371/journal.pone.0071328

1031 82. Zajc J, Liu Y, Dai W, Yang Z, Hu J, Gostinčar C, et al. Genome and transcriptome
1032 sequencing of the halophilic fungus *Wallemia ichthyophaga*: haloadaptations present and
1033 absent. BMC Genom. 2013;14: 617. doi:10.1186/1471-2164-14-617

1034 83. O'Kelly CJ, Farmer MA, Nerad TA. Ultrastructure of *Trimastix pyriformis* (Klebs) Bernard
1035 et al.: Similarities of *Trimastix* species with retortamonad and jakobid flagellates. Protist.
1036 1999;150: 149–162. doi:10.1016/S1434-4610(99)70018-0

1037 84. Mowbrey K, Dacks JB. Evolution and diversity of the Golgi body. FEBS Lett. 2009;583:
1038 3738–3745. doi:10.1016/j.febslet.2009.10.025

1039 85. Lee I, Tiwari N, Dunlop MH, Graham M, Liu X, Rothman JE. Membrane adhesion dictates
1040 Golgi stacking and cisternal morphology. Proc Natl Acad Sci USA. 2014;111: 1849–1854.
1041 doi:10.1073/pnas.1323895111

1042 86. Barlow LD, Nývltová E, Aguilar M, Tachezy J, Dacks JB. A sophisticated, differentiated
1043 Golgi in the ancestor of eukaryotes. BMC Biol. 2018;16: 27. doi:10.1186/s12915-018-0492-9

1044 87. Kulkarni-Gosavi P, Makhoul C, Gleeson PA. Form and function of the Golgi apparatus:
1045 scaffolds, cytoskeleton and signalling. FEBS Letters. 2019;593: 2289–2305.
1046 doi:10.1002/1873-3468.13567

1047 88. Boncompain G, Weigel AV. Transport and sorting in the Golgi complex: multiple
1048 mechanisms sort diverse cargo. Curr Opin Cell Biol. 2018;50: 94–101.
1049 doi:10.1016/j.ceb.2018.03.002

1050 89. Ahat E, Li J, Wang Y. New insights into the Golgi stacking proteins. Front Cell Dev Biol.
1051 2019;7: 131. doi:10.3389/fcell.2019.00131

1052 90. Li J, Ahat E, Wang Y. Golgi structure and function in health, stress, and diseases. The Golgi
1053 Apparatus and Centriole. Springer Cham; 2019. pp. 441–485.

1054 91. Park K, Ju S, Kim N, Park S-Y. The Golgi complex: a hub of the secretory pathway. BMB
1055 Rep. 2021;54: 246–252. doi:10.5483/BMBRep.2021.54.5.270

1056 92. Aridor M. A tango for coats and membranes: New insights into ER-to-Golgi traffic. Cell
1057 Reports. 2022;38: 110258. doi:10.1016/j.celrep.2021.110258

1058 93. Vargová R, Wideman JG, Derelle R, Klimeš V, Kahn RA, Dacks JB, et al. A eukaryote-wide
1059 perspective on the diversity and evolution of the ARF GTPase protein family. Genome Biol
1060 Evol. 2021;13: evab157. doi:10.1093/gbe/evab157

1061 94. Poinar GO. Description of an early Cretaceous termite (Isoptera: Kalotermitidae) and its
1062 associated intestinal protozoa, with comments on their co-evolution. Parasit Vectors. 2009;2:
1063 12. doi:10.1186/1756-3305-2-12

1064 95. Diamond LS. A new liquid medium for xenic cultivation of *Entamoeba histolytica* and other
1065 lumen-dwelling protozoa. J Parasitol. 1982;68: 958–959. doi:10.2307/3281016

1066 96. Bolger AM, Lohse M, Usadel B. Trimmomatic: a flexible trimmer for Illumina sequence
1067 data. Bioinformatics. 2014;30: 2114–2120. doi:10.1093/bioinformatics/btu170

1068 97. Koren S, Walenz BP, Berlin K, Miller JR, Bergman NH, Phillippy AM. Canu: scalable and
1069 accurate long-read assembly via adaptive k-mer weighting and repeat separation. Genome
1070 Res. 2017;27: 722–736. doi:10.1101/gr.215087.116

1071 98. Haddad I, Hiller K, Frimmersdorf E, Benkert B, Schomburg D, Jahn D. An emergent self-
1072 organizing map based analysis pipeline for comparative metabolome studies. In Silico Biol.
1073 2009;9: 163–178. doi:10.3233/ISB-2009-0396

1074 99. Treitli SC, Kolisko M, Husník F, Keeling PJ, Hampl V. Revealing the metabolic capacity of
1075 *Streblomastix strix* and its bacterial symbionts using single-cell metagenomics. Proc Natl
1076 Acad Sci USA. 2019;116: 19675–19684. doi:10.1073/pnas.1910793116

1077 100. Loman NJ, Quick J, Simpson JT. A complete bacterial genome assembled de novo using
1078 only nanopore sequencing data. Nat Methods. 2015;12: 733–735. doi:10.1038/nmeth.3444

1079 101. Walker BJ, Abeel T, Shea T, Priest M, Abouelliel A, Sakthikumar S, et al. Pilon: An
1080 Integrated Tool for Comprehensive Microbial Variant Detection and Genome Assembly
1081 Improvement. PLoS One. 2014;9: e112963. doi:10.1371/journal.pone.0112963

1082 102. Song L, Shankar DS, Florea L. Rascaf: Improving genome assembly with RNA
1083 sequencing data. Plant Genome. 2016;9: plantgenome2016.03.0027.
1084 doi:10.3835/plantgenome2016.03.0027

1085 103. Tarailo-Graovac M, Chen N. Using RepeatMasker to identify repetitive elements in
1086 genomic sequences. Curr Protoc Bioinformatics. 2009;Chapter 4: 4.10.1-4.10.14.
1087 doi:10.1002/0471250953.bi0410s25

1088 104. Stanke M, Waack S. Gene prediction with a hidden Markov model and a new intron
1089 submodel. Bioinformatics. 2003;19 Suppl 2: ii215-225. doi:10.1093/bioinformatics/btg1080

1090 105. Haas BJ, Delcher AL, Mount SM, Wortman JR, Smith RK, Hannick LI, et al. Improving
1091 the *Arabidopsis* genome annotation using maximal transcript alignment assemblies. Nucleic
1092 Acids Res. 2003;31: 5654–5666. doi:10.1093/nar/gkg770

1093 106. Haas BJ, Salzberg SL, Zhu W, Pertea M, Allen JE, Orvis J, et al. Automated eukaryotic
1094 gene structure annotation using EVidenceModeler and the Program to Assemble Spliced
1095 Alignments. Genome Biol. 2008;9: R7. doi:10.1186/gb-2008-9-1-r7

1096 107. Moriya Y, Itoh M, Okuda S, Yoshizawa AC, Kanehisa M. KAAS: an automatic genome
1097 annotation and pathway reconstruction server. Nucleic Acids Res. 2007;35: W182-185.
1098 doi:10.1093/nar/gkm321

1099 108. Eddy SR. Accelerated profile HMM searches. PLoS Comput Biol. 2011;7: e1002195.
1100 doi:10.1371/journal.pcbi.1002195

1101 109. Richter DJ, Berney C, Strassert JFH, Poh Y-P, Herman EK, Muñoz-Gómez SA, et al.
1102 EukProt: A database of genome-scale predicted proteins across the diversity of eukaryotes.
1103 Peer Community Journal. 2022;2: e56. doi:10.24072/pcjournal.173

1104 110. Heberle H, Meirelles GV, da Silva FR, Telles GP, Minghim R. InteractiVenn: a web-
1105 based tool for the analysis of sets through Venn diagrams. BMC Bioinformatics. 2015;16:
1106 169. doi:10.1186/s12859-015-0611-3

1107 111. Stechmann A, Hamblin K, Pérez-Brocal V, Gaston D, Richmond GS, van der Giezen M,
1108 et al. Organelles in *Blastocystis* that blur the distinction between mitochondria and
1109 hydrogenosomes. Curr Biol. 2008;18: 580–585. doi:10.1016/j.cub.2008.03.037

1110 112. Mi-ichi F, Abu Yousuf M, Nakada-Tsukui K, Nozaki T. Mitosomes in *Entamoeba*
1111 *histolytica* contain a sulfate activation pathway. Proc Natl Acad Sci U S A. 2009;106: 21731–
1112 21736. doi:10.1073/pnas.0907106106

1113 113. Barberà MJ, Ruiz-Trillo I, Tufts JYA, Bery A, Silberman JD, Roger AJ. *Sawyeria*
1114 *marylandensis* (Heterolobosea) has a hydrogenosome with novel metabolic properties.
1115 Eukaryot Cell. 2010;9: 1913–1924. doi:10.1128/EC.00122-10

1116 114. Alcock F, Webb CT, Dolezal P, Hewitt V, Shingu-Vasquez M, Likić VA, et al. A small
1117 Tim homohexamer in the relict mitochondrion of *Cryptosporidium*. Mol Biol Evol. 2012;29:
1118 113–122. doi:10.1093/molbev/msr165

1119 115. Noguchi F, Shimamura S, Nakayama T, Yazaki E, Yabuki A, Hashimoto T, et al.
1120 Metabolic capacity of mitochondrion-related organelles in the free-living anaerobic
1121 stramenopile *Cantina marsupialis*. Protist. 2015;166: 534–550.
1122 doi:10.1016/j.protis.2015.08.002

1123 116. Pyrihová E, Motyčková A, Voleman L, Wandyszewska N, Fišer R, Seydlová G, et al. A
1124 single Tim translocase in the mitosomes of *Giardia intestinalis* illustrates convergence of
1125 protein import machines in anaerobic Eukaryotes. Genome Biol Evol. 2018;10: 2813–2822.
1126 doi:10.1093/gbe/evy215

1127 117. Emanuelsson O, Brunak S, von Heijne G, Nielsen H. Locating proteins in the cell using
1128 TargetP, SignalP and related tools. Nat Protoc. 2007;2: 953–971. doi:10.1038/nprot.2007.131

1129 118. Fukasawa Y, Tsuji J, Fu S-C, Tomii K, Horton P, Imai K. MitoFates: improved prediction
1130 of mitochondrial targeting sequences and their cleavage sites. Mol Cell Proteomics. 2015;14:
1131 1113–1126. doi:10.1074/mcp.M114.043083

1132 119. Krogh A, Larsson B, von Heijne G, Sonnhammer EL. Predicting transmembrane protein
1133 topology with a hidden Markov model: application to complete genomes. J Mol Biol.
1134 2001;305: 567–580. doi:10.1006/jmbi.2000.4315

1135 120. Imai K, Fujita N, Gromiha MM, Horton P. Eukaryote-wide sequence analysis of
1136 mitochondrial β-barrel outer membrane proteins. BMC Genom. 2011;12: 79.
1137 doi:10.1186/1471-2164-12-79

1138 121. McGuffin LJ, Bryson K, Jones DT. The PSIPRED protein structure prediction server.
1139 Bioinformatics. 2000;16: 404–405. doi:10.1093/bioinformatics/16.4.404

1140 122. Aslett M, Aurrecoechea C, Berriman M, Brestelli J, Brunk BP, Carrington M, et al.
1141 TriTrypDB: a functional genomic resource for the Trypanosomatidae. Nucleic Acids Res.
1142 2010;38: D457-462. doi:10.1093/nar/gkp851

1143 123. UniProt Consortium. UniProt: a worldwide hub of protein knowledge. Nucleic Acids Res.
1144 2019;47: D506–D515. doi:10.1093/nar/gky1049

1145 124. Nguyen L-T, Schmidt HA, von Haeseler A, Minh BQ. IQ-TREE: A fast and effective
1146 stochastic algorithm for estimating maximum-likelihood phylogenies. Mol Biol Evol.
1147 2015;32: 268–274. doi:10.1093/molbev/msu300

1148 125. Valasatava Y, Rosato A, Banci L, Andreini C. MetalPredator: a web server to predict
1149 iron–sulfur cluster binding proteomes. Bioinformatics. 2016;32: 2850–2852.
1150 doi:10.1093/bioinformatics/btw238

1151 126. Blum M, Chang H-Y, Chuguransky S, Grego T, Kandasaamy S, Mitchell A, et al. The
1152 InterPro protein families and domains database: 20 years on. Nucleic Acids Res. 2021;49:
1153 D344–D354. doi:10.1093/nar/gkaa977

1154 127. Kanehisa M, Sato Y, Morishima K. BlastKOALA and GhostKOALA: KEGG tools for
1155 functional characterization of genome and metagenome sequences. J Mol Biol. 2016;428:
1156 726–731. doi:10.1016/j.jmb.2015.11.006

1157 128. Emms DM, Kelly S. OrthoFinder: phylogenetic orthology inference for comparative
1158 genomics. Genome Biol. 2019;20: 238. doi:10.1186/s13059-019-1832-y

1159 129. Zimmermann L, Stephens A, Nam S-Z, Rau D, Kübler J, Lozajic M, et al. A completely
1160 reimplemented MPI bioinformatics toolkit with a new HHpred server at its core. J Mol Biol.
1161 2018;430: 2237–2243. doi:10.1016/j.jmb.2017.12.007

1162 130. Capella-Gutiérrez S, Silla-Martínez JM, Gabaldón T. trimAl: a tool for automated
1163 alignment trimming in large-scale phylogenetic analyses. Bioinformatics. 2009;25: 1972–
1164 1973. doi:10.1093/bioinformatics/btp348

1165 131. Stamatakis A. RAxML version 8: a tool for phylogenetic analysis and post-analysis of
1166 large phylogenies. Bioinformatics. 2014;30: 1312–1313. doi:10.1093/bioinformatics/btu033

1167 132. Miller MA, Pfeiffer W, Schwartz T. Creating the CIPRES Science Gateway for inference
1168 of large phylogenetic trees. 2010 Gateway Computing Environments Workshop (GCE).
1169 2010. pp. 1–8. doi:10.1109/GCE.2010.5676129

1170 133. Hirst J, Schlacht A, Norcott JP, Traynor D, Bloomfield G, Antrobus R, et al.
1171 Characterization of TSET, an ancient and widespread membrane trafficking complex. Elife.
1172 2014;3: e02866. doi:10.7554/eLife.02866

1173 134. Klinger CM, Klute MJ, Dacks JB. Comparative genomic analysis of multi-subunit
1174 tethering complexes demonstrates an ancient pan-eukaryotic complement and sculpting in
1175 Apicomplexa. PLoS One. 2013;8: e76278. doi:10.1371/journal.pone.0076278

1176 135. Tang S, Lomsadze A, Borodovsky M. Identification of protein coding regions in RNA
1177 transcripts. Nucleic Acids Res. 2015;43: e78. doi:10.1093/nar/gkv227

1178 136. Edgar RC. MUSCLE: multiple sequence alignment with high accuracy and high
1179 throughput. Nucleic Acids Res. 2004;32: 1792–1797. doi:10.1093/nar/gkh340

1180 137. Stamatakis A. RAxML-VI-HPC: maximum likelihood-based phylogenetic analyses with
1181 thousands of taxa and mixed models. Bioinformatics. 2006;22: 2688–2690.
1182 doi:10.1093/bioinformatics/btl446

1183 138. Abascal F, Zardoya R, Posada D. ProtTest: selection of best-fit models of protein
1184 evolution. Bioinformatics. 2005;21: 2104–2105. doi:10.1093/bioinformatics/bti263

1185 139. Felsenstein J. PHYLIP-Phylogeny inference package (Version 3.2). Cladistics. 1989;5:
1186 164–166. doi:10.1111/j.1096-0031.1989.tb00562.x

1187 140. Huelsenbeck JP, Ronquist F. MRBAYES: Bayesian inference of phylogenetic trees.
1188 Bioinformatics. 2001;17: 754–755. doi:10.1093/bioinformatics/17.8.754

1189

1190 # Tables

1191 **Table 1. General features of the Preaxostyla genomes discussed in this study**

Sample	Scaffolds	Total length (bp)	N50 (kbp)	Completeness (%; BUSCO odb9)	Completeness (%; Merqury)	G+C content (%)	Protein-Coding Loci	Source
P. pyriformis	633	56,627,582	276.6	76.3	94.01	60.94	10,815	NCBI JAPMOS000000000
B. nauphoetae	879	88,537,989	199.5	76.6	98.24	44.96	25,221	NCBI JARBJD000000000
M. exilis	2,092	74,712,536	71.44	75.3	n/a	36.8	16,768	GiardiaDB release 46 GiardiaDB-46_MexilisPA203
S. strix	50,889	152,152,197	5.18	69.6	n/a	26.6	56,706	NCBI SNRW00000000

1192

1193

1194 # Figure legends

1195 **Fig 1. Summary of the searches for proteins physically associated with MROs.** (A) Schematic
1196 representation of the position of Preaxostyla in the eukaryotic tree of life and the topology within
1197 the group. Representative non-preaxostylan organism silhouettes are from PhyloPic (phylopic.org).
1198 (B) Results of fours searches for putative mitochondrial proteins are summarized and species are
1199 color-coded as in A. Detailed information on the three steps of the searches and candidates is given
1200 in S2 File. (C) Mitochondrion hallmark proteins detected in the data sets of *P. pyriformis* and
1201 *T. marina* are shown in blue/green. No such candidate was recovered for any oxymonad
1202 representative.

1203 **Fig 2. Hypothetical reconstruction of the extended glycolysis in Preaxostyla.** Bold outline
1204 indicates alternative glycolytic enzymes. Abbreviations and Enzyme Commission numbers are
1205 given in S6 File. Presence of the enzymes in Preaxostyla data sets is indicated by a color code.

1206 **Fig 3. Phylogenetic relationship among hydrogenases of Preaxostyla.** (A) Schematic
1207 representation of domain architectures of hydrogenases in Preaxostyla species. HydA: [FeFe]
1208 hydrogenase; CysJ: NADPH-dependent sulfite reductase; NuoG: NADH-quinone oxidoreductase.
1209 (B) Detailed view of the part of a hydrogenase phylogenetic tree that corresponds to a clade
1210 including long hydrogenases. The domain architecture of the proteins is indicated by color bars.
1211 The full tree is given in S4D File.

1212 **Fig 4. Complement of Golgi-associated proteins in Preaxostyla.** This Coulson plot shows the
1213 set of proteins present in the Preaxostyla predicted proteomes. Empty segments denote failure to
1214 identity a candidate orthologue, while filled segments denote success, with paralog numbers inset
1215 as relevant. Candidate proteins are identified by homology-searching and verified by phylogenetics

1216 as relevant. Details are given in S6 File.

1217 Supplementary figure legends

1218 **S1 Fig. Hypothetical map of the amino acid metabolism in *P. pyriformis*.** Brown color indicates
1219 enzymes possibly involved in amino acid biosynthesis pathways. Red color indicates enzymes
1220 possibly involved in ATP production. Note that some of the connections between metabolites
1221 correspond to the mere transfer of the amino group rather than conversion of the carbon backbone
1222 of the molecule (green color). Cyan color is used for remaining enzymes. Abbreviations and
1223 Enzyme Commission numbers are given in S6 File.

1224 **S2 Fig. Hypothetical map of the amino acid metabolism in *T. marina*.** Brown color indicates
1225 enzymes possibly involved in amino acid biosynthesis pathways. Red color indicates enzymes
1226 possibly involved in ATP production. Note that some of the connections between metabolites
1227 correspond to the mere transfer of the amino group rather than conversion of the carbon backbone
1228 of the molecule (green color). Cyan color is used for remaining enzymes. Abbreviations and
1229 Enzyme Commission numbers are given in S6 File.

1230 **S3 Fig. Hypothetical map of the amino acid metabolism in *M. exilis*, *B. nauphoetae*, and**
1231 ***S. strix*.** Brown color indicates enzymes possibly involved in amino acid biosynthesis pathways.
1232 Red color indicates enzymes possibly involved in ATP production. Note that some of the
1233 connections between metabolites correspond to the mere transfer of the amino group rather than

1234 conversion of the carbon backbone of the molecule (green color). Cyan color is used for remaining
1235 enzymes. Abbreviations and Enzyme Commission numbers are given in S6 File.

1236 **S4 Fig. Venn diagram showing the distribution of orthologous groups (OGs) of Fe-S cluster-**
1237 **containing proteins among the species of Preaxostyla.** The identity of the OGs and of the
1238 component proteins are provided in S7 File.

1239 Supplementary files

1240 **S1 File. Genome completeness analyses.**

1241 **S2 File. Results of searches for mitochondrial candidates in Preaxostyla.**

1242 **S3 File. Orthologous groups analysis.**

1243 **S4 File. Phylogenetic trees of selected genes individually discussed in this work.**

1244 **S5 File. Phylogenetic trees of mitochondrial candidates.**

1245 **S6 File. Manual annotation of protein-coding genes in Preaxostyla.**

1246 **S7 File. Results of searches for FeS-cluster containing proteins in Preaxostyla.**

1247 **S8 File. Results of searches for peroxins in Preaxostyla.**

1248 **S9 File. Results of searches for transmembrane transporters in Preaxostyla.**

A

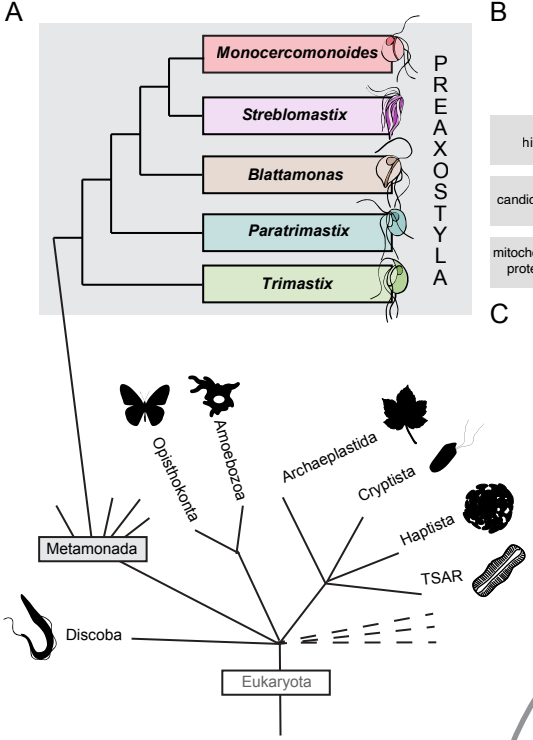

B

	1					2					3					4				
	mitochondrial import machinery					proteins with localisation signal					MOM targeted TA-proteins					β-barrel MOM proteins				
	homology search by HMMER					signal prediction by TargetP and MitoFates					short transmembrane domain flanked from both sides by positively charged residues					presence of C-terminal β-signal				
hits	63	50	53	37	22	83	248	2	201	141	100	134	475	81	25	57	121	101	23	6
candidates	13	12	8	16	8	12	9	0	19	31	5	9	9	12	9	1	1	2	1	2
mitochondrial proteins	0	0	0	10	2	0	0	0	0	3	0	0	0	0	1	0	0	0	1	0

C

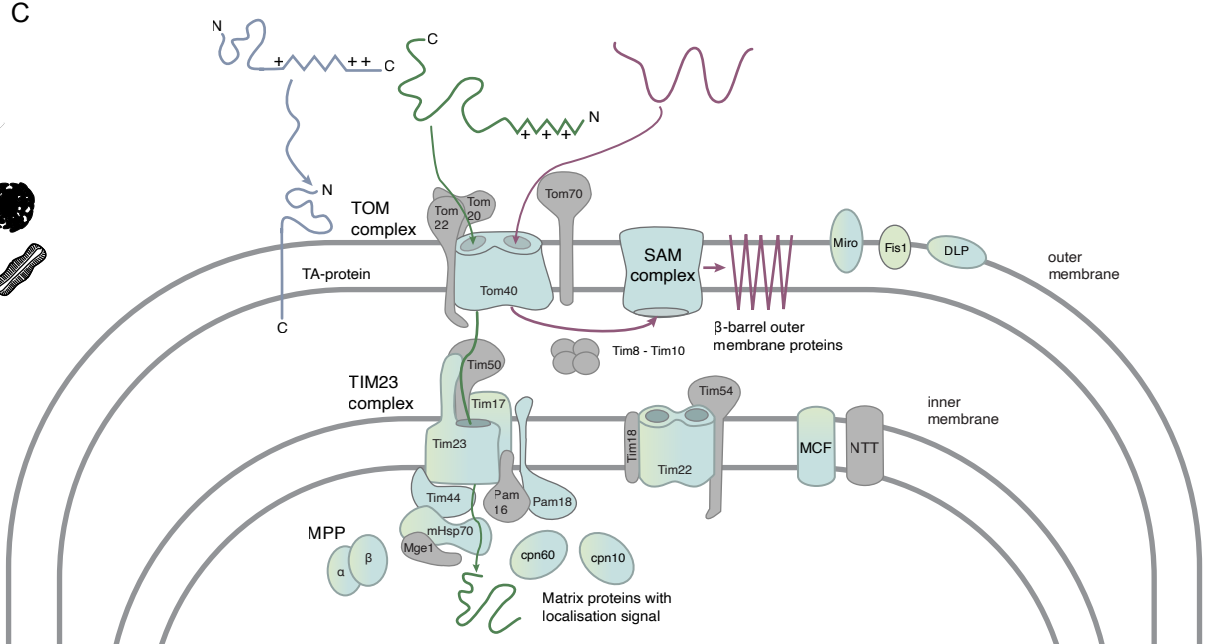

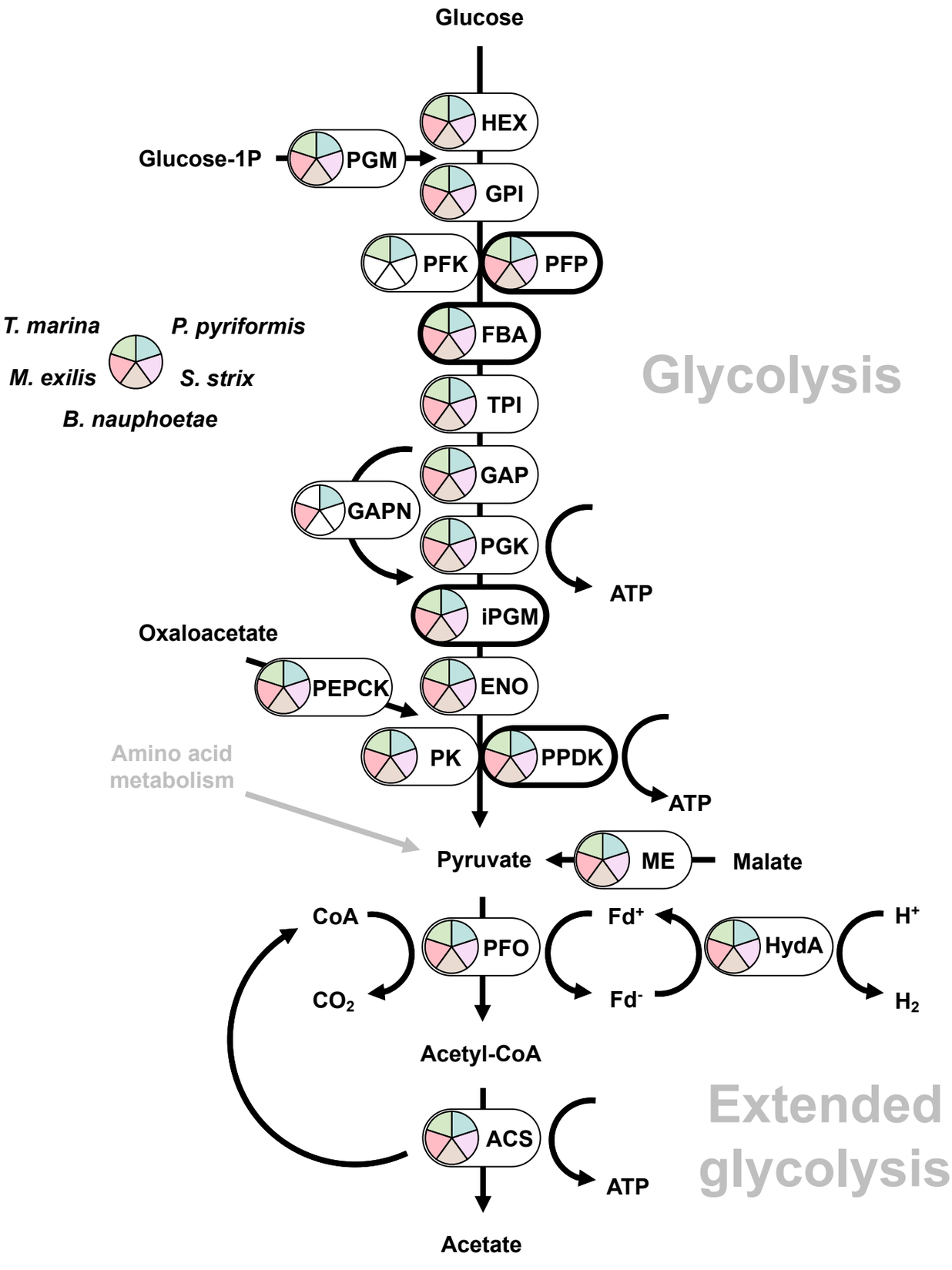
Glucose
HEX
Glucose-1P
PGM
GPI
PFK
PFP
T. marina
P. pyriformis
M. exilis
S. strix
B. nauphoetae
FBA
Glycolysis
TPI
GAP
GAPN
PGK
ATP
iPGM
Oxaloacetate
PEPCK
ENO
Amino acid metabolism
PK
PPDK
ATP
Pyruvate
ME
Malate
CoA
PFO
Fd+
HydA
H+
CO2
Fd-
H2
Acetyl-CoA
ACS
ATP
Extended glycolysis
Acetate

A

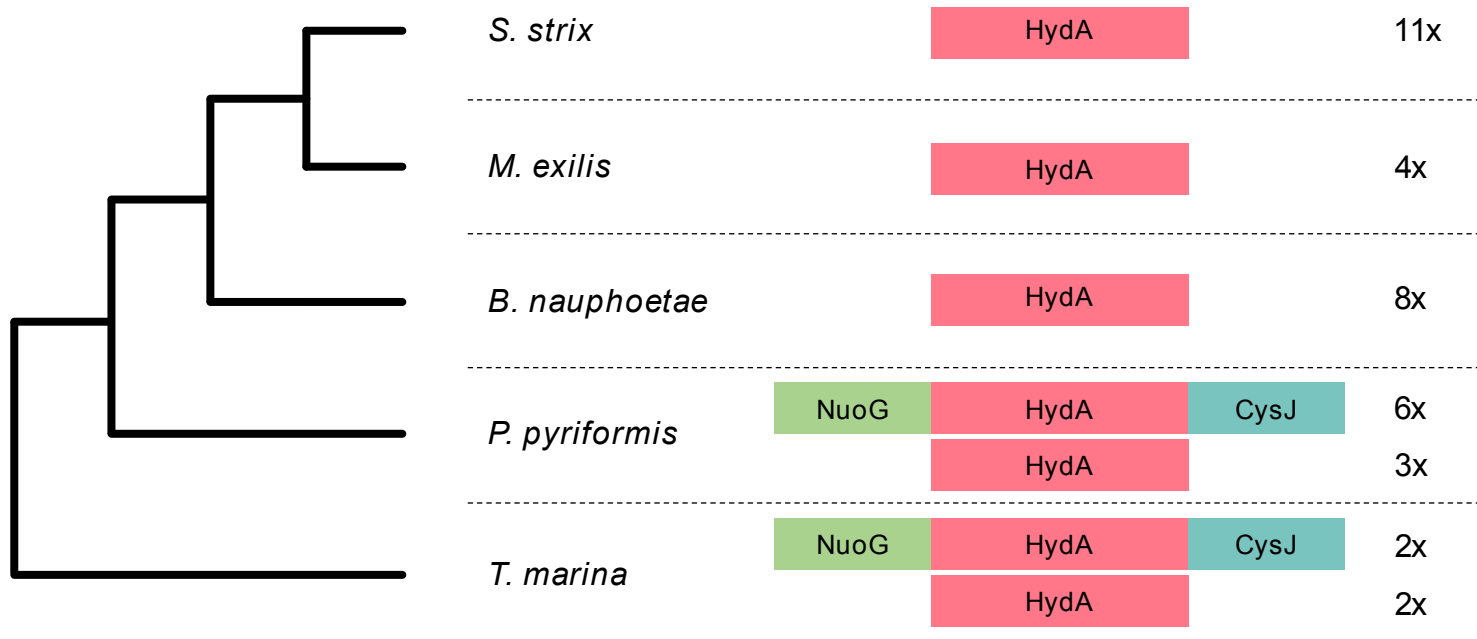
S. strix
HydA
11x
M. exilis
HydA
4x
B. nauphoetae
HydA
8x
P. pyriformis
NuoG
HydA
CysJ
6x
HydA
3x
T. marina
NuoG
HydA
CysJ
2x
HydA
2x

B

Dysnectes brevis EP00768 P001904
Chilomastix cuspidata EP00767 P0026808
Chilomastix cuspidata EP00767 P000227
Chilomastix cuspidata EP00767 P008182
Dysnectes brevis EP00768 P003997
Carpediemonas membranifera EP01146 P006601
Carpediemonas membranifera KAG9394831.1
Aduncisulcus paluster GKT24525.1
Pygsuia biforma EP00033 P007230
Pygsuia biforma EP00033 P000096
Tritrichomonas foetus EP00706 P011172
Trichomonas vaginalis XP_001580488.1
Trichomonas vaginalis EP00705 P045848
Trichomonas vaginalis XP_001328981.1
Trichomonas vaginalis XP_001580286.1
Pseudotrichonympha grassii BAF82035.1
Pygsuia biforma EP00033 P008592
Blastocystis hominis XP_012899174.1
Blastocystis sp. ACD10930.1
Pygsuia biforma EP00033 P007207
Mastigamoeba balamuthi AGA37391.1
Stygiella incarcerata ANM86869.1
Stygiella incarcerata ANM86868.1
Paratrimastix pyriformis PAPYR_1278
Paratrimastix pyriformis PAPYR_1296
Paratrimastix pyriformis PAPYR_1254
Trimastix marina Gene.1507::gnl|Trimastix_PCT|547
Mastigamoeba balamuthi AGA37394.1
Paratrimastix pyriformis PAPYR_8530
Paratrimastix pyriformis PAPYR_8536
Paratrimastix pyriformis PAPYR_8532
Trimastix marina Gene.6882::gnl|Trimastix_PCT|2098

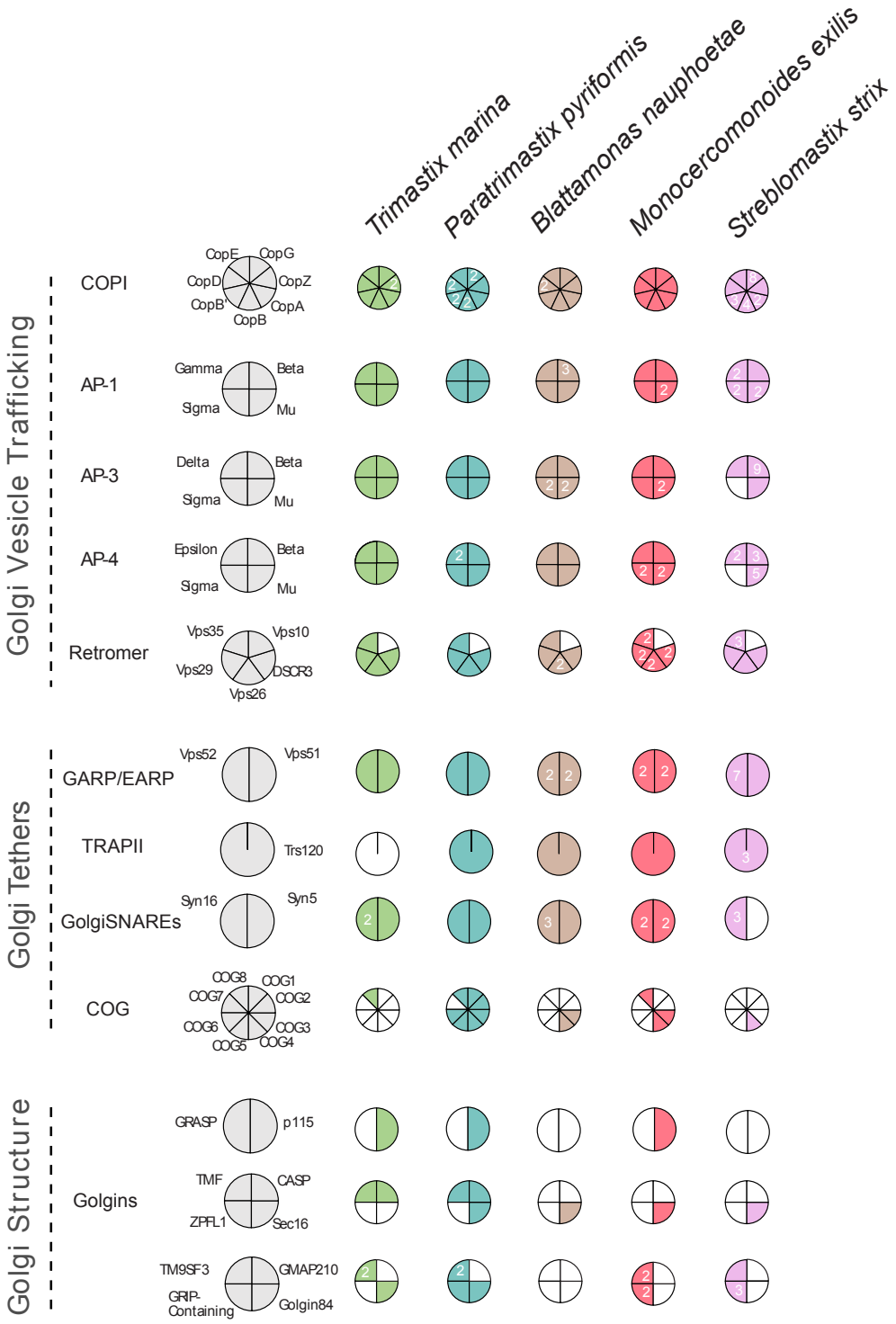
Trimastix marina
Paratrimastix pyriformis
Blattamonas nauphoetae
Monocercomonoides exilis
Streblomastix strix
Golgi Vesicle Trafficking
COPI
CopE
CopG
CopD
CopZ
CopB'
CopA
CopB
AP-1
Gamma
Beta
Sigma
Mu
AP-3
Delta
Beta
Sigma
Mu
AP-4
Epsilon
Beta
Sigma
Mu
Retromer
Vps35
Vps10
Vps29
DSCR3
Vps26
Golgi Tethers
GARP/EARP
Vps52
Vps51
TRAPII
Trs120
GolgiSNAREs
Syn16
Syn5
COG
COG8
COG1
COG7
COG2
COG6
COG3
COG5
COG4
Golgi Structure
Golgins
GRASP
p115
TMF
CASP
ZPFL1
Sec16
TM9SF3
GMAP210
GRIP-Containing
Golgin84